

CONTROL IN STRESS DEVELOPMENT IN BONE

by

YSSA DeWOODY, B.S., M.S.

A DISSERTATION


IN

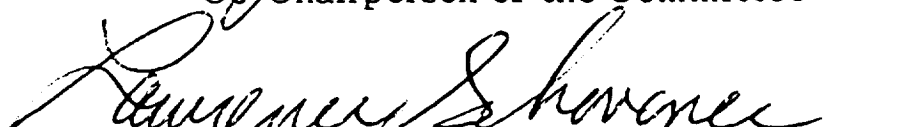
MATHEMATICS

Submitted to the Graduate Faculty  
of Texas Tech University in  
Partial Fulfillment of  
the Requirements for  
the Degree of

DOCTOR OF PHILOSOPHY

Approved

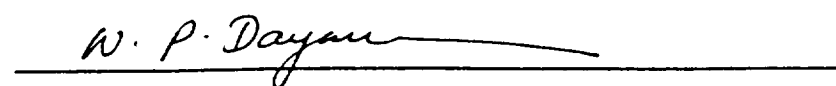
  
Co-Chairperson of the Committee

  
Co-Chairperson of the Committee

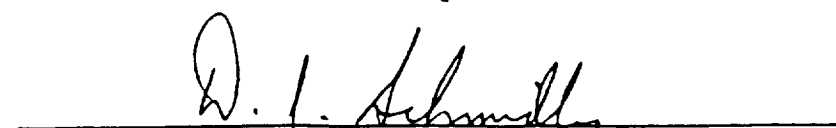




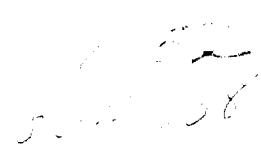




Accepted

  
Dean of the Graduate School

NAG-2-899  
382274



## ACKNOWLEDGMENTS

I am most grateful to my loving husband, Andrew DeWoody. His overwhelming confidence in me continues to be a driving force in both my personal and professional life. Words cannot express the joy you have added to my life. I thank you for all your love, support and patience.

I would especially like to thank the co-chairs of my committee: Clyde Martin and Lawrence Schovanec. This dissertation has been improved greatly due to their support and guidance. I have a great deal of respect for both men and consider it a blessing to have worked with them. A special thanks to Clyde Martin for giving me numerous opportunities to travel and expand my horizons. His thoughtfulness and kindness will be remembered fondly. I owe a debt of gratitude to Lawrence Schovanec. He went beyond the call of duty to help me with this dissertation and especially in the distribution of the copies to my committee member; this could not be more appreciated.

While at Texas Tech University, I have had the opportunity to meet a host of great people. Some of these people have been my teachers, some have been my mentors and some my friends. All of these people have enriched my life and I am grateful for the opportunity of knowing them.

I would also like to thanks the Helen Hodges Foundation, ARCS, and the Graduate School for the financial support they have given me through scholarships, fellowships and summer research grants.

# CONTENTS

ACKNOWLEDGMENTS . . . . .	ii
ABSTRACT . . . . .	v
LIST OF TABLES . . . . .	vi
LIST OF FIGURES . . . . .	vii
I. INTRODUCTION . . . . .	1
II. JUSTIFICATION OF THE APPROACH . . . . .	3
2.1 Introduction . . . . .	3
2.2 Inverse-Dynamics . . . . .	3
2.3 Direct-Dynamics . . . . .	5
III. MUSCULOTENDON COMPLEX . . . . .	7
3.1 Architecture of Musculotendon . . . . .	7
3.2 Functional Properties of the Musculotendon . . . . .	8
3.2.1 Force-Length Properties of Muscle . . . . .	8
3.2.2 Force-Velocity Properties of Muscle . . . . .	11
3.2.3 Force-Length Properties of Tendon . . . . .	12
IV. MUSCULOTENDON DYNAMIC MODEL . . . . .	15
4.1 Introduction . . . . .	15
4.2 Musculotendon Contraction Dynamics . . . . .	15
4.2.1 Scaling and Curves . . . . .	15
4.2.2 Derivation of Contraction Dynamics of Musculotendon Unit . . . . .	21
4.3 Activation Dynamics . . . . .	24
V. THE MUSCULOSKELETAL MODEL . . . . .	27
5.1 Introduction . . . . .	27
5.2 Skeletal Model . . . . .	27
5.3 Passive Constraints at the Joints . . . . .	32
5.4 Soft Floor Constraints . . . . .	35
5.5 Incorporating the Musculotendon Actuators . . . . .	36
5.5.1 Minimal Set of Muscles . . . . .	36
5.5.2 Origins and Insertions . . . . .	36

5.5.3	Calculation of Musculotendon Length, Velocity and Moment Arm . . . . .	41
5.6	Controls for the Musculotendon Actuators . . . . .	45
VI.	DYNAMIC SIMULATIONS . . . . .	47
6.1	Numerical Implementation . . . . .	47
6.2	Dynamic Simulation . . . . .	50
6.2.1	Controls and Initial Conditions . . . . .	50
6.2.2	Joint Angles and Joint Torques . . . . .	53
6.2.3	Musculotendon Analysis . . . . .	55
VII.	A CONTINUUM ANALYSIS OF SKELETAL ELEMENTS . . . .	66
7.1	Introduction to Bone Mechanics . . . . .	66
7.2	Finite Element Analysis of Tibia . . . . .	69
VIII.	CONCLUSIONS . . . . .	73
	BIBLIOGRAPHY . . . . .	76
	APPENDIX: AUTOLEV CODE . . . . .	82

## ABSTRACT

The role of forces produced by the musculotendon units in the stress development of the long bones during gait has not been fully analyzed. It is well known that the musculotendons act as actuators producing the joint torques which drive the body. Although the joint torques required to perform certain motor tasks can be recovered through a kinematic analysis, it remains a difficult problem to determine the actual forces produced by each muscle that resulted in these torques. As a consequence, few studies have focused on the role of individual muscles in the development of stress in the bone.

This study takes a control theoretic approach to the problem. A seven-link, eight degrees of freedom model of the body is controlled by various muscle groups on each leg to simulate gait. The simulations incorporate Hill-type models of muscles with activation and contraction dynamics controlled through neural inputs. This direct approach allows one to know the exact muscle forces exerted by each musculotendon throughout the gait cycle as well the joint torques and reaction forces at the ankle and knee. Stress and strain computed by finite element analysis on skeletal members will be related to these derived loading conditions. Thus the role of musculoskeletal dynamics and neuromuscular control in the stress development of the tibia during gait can be analyzed.

## LIST OF TABLES

5.1	Segment Dimensions and Inertial Parameters . . . . .	30
5.2	Coefficients for Passive Joint Moments . . . . .	34
5.3	Musculotendon Groups and Their Constituent Muscles . . . . .	37
5.4	Parameters Defining the Musculotendon Actuators . . . . .	38
5.5	Origins and Insertions of the Musculotendon Groups . . . . .	40
6.1	Initial Conditions for the Gait Simulation . . . . .	54

## LIST OF FIGURES

3.1	Geometry of Pennated Muscle . . . . .	8
3.2	Organization of Striated Muscle . . . . .	9
3.3	Isometric Force-Length Relation for Muscle . . . . .	10
3.4	Active Tension-Length Curve for Muscles . . . . .	11
3.5	Force-Velocity Relation for Muscles . . . . .	13
3.6	Force-Length-Velocity Surface for Muscles . . . . .	13
3.7	Nominal Stress-Strain Curve for Tendons . . . . .	14
4.1	Block Diagram of the Coupled Dynamical Systems . . . . .	16
4.2	Isometric Passive Force-Length for Muscles . . . . .	18
4.3	Isometric Active Force-Length for Muscles . . . . .	18
4.4	Inverse Force-Velocity Relation for Muscles . . . . .	19
4.5	Generic Force-Strain Relation for Tendons . . . . .	20
4.6	Force-Strain Relation for Tendons . . . . .	21
4.7	Hill Type Model of the Musculotendon . . . . .	22
4.8	Activation Dynamics . . . . .	26
5.1	3-D, 8 DOF Model Showing Segment Angle Definitions . . . . .	28
5.2	Definition for Inertial and Segmental Parameters . . . . .	29
5.3	Simulated Gait Cycle With Respect to Total Gait Cycle . . . . .	31
5.4	Passive Joint Moment for Ankle Joint . . . . .	32
5.5	Passive Joint Moment for Knee Joint . . . . .	33
5.6	Passive Joint Moment for Hip Joint . . . . .	33
5.7	“Soft” Constraint on Swing Leg During Double Support . . . . .	35
5.8	Minimal Set of Ten Musculotendon Actuators . . . . .	39
5.9	Definitions for the Foot, Tibial, Femoral and Pelvic Frames . . . . .	41
5.10	Muscle Pathway and Effective Moment Arm . . . . .	43
5.11	Effective Moment Arm of Vasti . . . . .	44
5.12	Effective Moment Arm of Hamstring . . . . .	44

5.13	Effective Moment Arm of Gastrocnemius . . . . .	44
5.14	Controls and Activation Patterns Used by Yamaguchi . . . . .	46
6.1	2-Dimensional Representation of Our Gait Simulation . . . . .	50
6.2	Controls Utilized in Simulation . . . . .	52
6.3	Joint Angle Definitions . . . . .	55
6.4	Joint Trajectories . . . . .	56
6.5	Stance Ankle Joint Torque . . . . .	57
6.6	Stance Knee Joint Torque . . . . .	58
6.7	Stance Hip Joint Torque for Flexion . . . . .	59
6.8	Stance Hip Joint Torque for Abduction . . . . .	60
6.9	Swing Ankle Joint Torque . . . . .	60
6.10	Swing Knee Joint Torque . . . . .	61
6.11	Swing Hip Joint Torque . . . . .	62
6.12	Normalized Force Histories for each Musculotendon . . . . .	64
6.13	Normalized Power Curves for each Musculotendon . . . . .	65
7.1	Axial Stress Induced During Flat Foot . . . . .	71
7.2	Axial Stress Induced During Heel Strike . . . . .	72



## CHAPTER I

### INTRODUCTION

The study of stress development in bone is an active area of research which is relevant to the prediction and prevention of injury. Stress fractures have been a recurring problem with military recruits during intense training and are now being seen more frequently in civilian athletes (Sharkey *et al.*, 1995). The need to better understand the development of these fractures is a driving force behind this research. While the problems being addressed by this research are typically thought to reside in the fields of biomechanics or bioengineering, mathematics is central to the formulation and solution of these problems. In particular, control theory, fracture mechanics and numerical analysis are especially relevant in the approach developed in this investigation.

Before issues such as failure of bone can be addressed, one needs to have a good understanding of the stress fields incurred in bone throughout tasks which are deemed normal. The integrity of the calculated stress fields during a task will ultimately depend not only on the accuracy of the model describing the material properties of bone but also on the proper interpretation and calculation of the loading conditions to which the bone is subjected. Defining the loading conditions which accurately reflect the state of a human bone during *in vivo* activity is a challenge due to the ethical limitations inherent in working with human subjects. The practicality of utilizing strain gauges bonded to the bone and other such monitoring devices is restricted due to the risk of infection and discomfort imposed on the subject. Thus non-invasive techniques are highly recommended.

One of the goals of this research is to develop an analytical, predictive method for acquiring appropriate dynamic loading conditions for the long bones of humans throughout the gait cycle. Such an analytical model would provide information that might otherwise be obtained only through invasive procedures. A promising approach to this problem lies in the forward analysis of a mathematical model capable of simulating normal gait which incorporates the interaction of the active and passive structures of the body. Muscles are the active force producing components in the body while tendons, ligaments and bones are representative of

the passive structures. Although anatomic considerations imply the importance of considering the interaction between these structures, most studies in the past have concentrated on the behavior of these elements in isolation. Studies have shown that ligaments and bones behave differently in isolation by storing more energy, requiring more force to rupture, and sustaining increased elongation as the speed of loading is increased (Wainwright *et al.*, 1976). It is also hypothesized that stress fractures in bone represent either a failure of fatigued muscles to absorb impact (Markey, 1989) or are the result of uncoordinated muscular action (Lanyon, 1984). Thus a reliable mathematical model must incorporate the combined effects of the muscle-tendon-ligament-bone complex by considering both active and passive structures as biological control systems.

Deriving loading conditions from a simulation is a relatively new procedure and a challenging modeling problem. Chapter II will emphasize advantages of this method. Chapters III and IV are devoted to the modeling of musculotendons. A great deal of importance is placed on the proper modeling of the musculotendons for two reasons. First, since the musculotendons are known to actuate the body, any model of gait which hopes to mimic nature must include a fairly accurate description of muscle. Secondly, it is a contention of this research that the musculotendons play a major role in defining appropriate loading conditions of the bone. Since the validity of the loading conditions relies on the ability of the model to simulate normal gait as accurately as possible, Chapters V and VI will concentrate on the development of the musculoskeletal model, the incorporation of the musculotendon actuators, and the implementation of the simulations. Thus a major portion of this dissertation is devoted to defining and validating a model through which appropriate loading conditions can be derived.

The last portion of this dissertation will involve a finite element analysis of the tibia using the derived loading conditions. The effects of musculature in the loading conditions will be emphasized. These computations demonstrate how loading conditions from a forward analysis may be implemented in a stress analysis. More importantly, the results will indicate that the incorporation of both active and passive structures of the body are essential in accurately predicting the state of stress in the long bones of the lower extremities.

## CHAPTER II

### JUSTIFICATION OF THE APPROACH

#### 2.1 Introduction

To study the stress and strain distribution on the long bones, one must know the loading conditions. The relevant static loading conditions used in the past include joint reaction forces, joint torques, bending moments, and in some cases estimations of individual muscle forces. The question to be addressed in this section is what type of analysis provides a good methodology for studying the effects of different loading conditions associated with various forms of gait.

Typically the body is modeled as a multi-link object in this sort of analysis. If the model has  $n$  degrees of freedom (dof), then the equations of motion governing this object can be written in the following simple form

$$M\ddot{\theta} = T + V + G + E \quad (2.1)$$

where  $\ddot{\theta}$  is a  $n \times 1$  vector containing segmental acceleration,  $M$  is the  $n \times n$  "mass matrix," and  $T, V, G, E$  are  $n \times 1$  vectors representing the internal segmental torques, inertial, gravitational, and external forces acting on the body. Once these equations are derived, there are essentially two approaches in finding the loading conditions derived from a certain motor task: an inverse-dynamic approach or a direct-dynamic approach.

#### 2.2 Inverse-Dynamics

Inverse-dynamics is an approach that proceeds in a backwards manner, taking observed motions and then deriving from these motions the joint torques responsible. Thus motion acts as the input in this method and joint torques are the output. It is convenient to write equation (2.1) in the following form

$$T = (M\ddot{\theta} - V - G - E)$$

to emphasize the dependence of  $T$  on the body trajectories. This approach requires experimental, kinematic data, i.e., ground reaction forces, mass and inertial

characteristics of segments, and observed motions. If these kinematic variables are assumed to be known functions of time, the set of differential equations of motion becomes algebraic and joint torques are easily computed (King, 1984).

Although joint torques are easily derived, it is a nontrivial matter to discern the distribution of force among the muscles from this data. As Davy and Audu (1987) stated, "There are typically more unknown forces than can be determined in the equipollence relations between resultant and individual member force (Crowninshield, 1978; Penrod *et al.*, 1974), so muscle forces can not be determined directly from mechanical relations alone." This is referred to as the "redundancy problem." Typically the muscle set is reduced by grouping muscles of similar function (Patriarco, 1981) and by using EMG activity as a guide in determining which muscles were used during the motor task (King, 1984; Biewener, 1992). If the problem is still indeterminate, then an optimization scheme is usually utilized; however the selection of appropriate optimization criterion or the construction of proper cost functions remains disputed (King, 1984). Some cost functions which have been used in the past include the sum of muscle forces (Seireg and Arvikar, 1973; Penrod *et al.*, 1974), the sum of muscle stresses or a related quantity (Crowninshield, 1978; Crowninshield and Brand, 1981), and energy expenditure rate (Hardt, 1978; Patriarco *et al.*, 1978). All the works cited above included no excitation nor contraction dynamics of the muscles, and thus are referred to as *static optimization* after Hardt(1978). Depending on the form of the cost function, the optimization problem is solved via linear programming, gradient-restoration algorithms, or another appropriate method (Davy and Audu, 1987).

There are several shortcomings associated with static optimization. These methods neglect the role of muscle dynamics and assume that muscle actions at any instant are independent of action at all other points (Davy and Audu, 1987). Neglecting muscle dynamics often results in muscle force histories which are discontinuous in time (Yamaguchi, 1990). Furthermore, the results from static optimization are highly dependent on the cost function selected which sometimes predict physiologically unrealistic results (Hardt, 1978; Seireg and Arvikar, 1975). Adding physiological constraint equations can help prevent some of these unrealistic results (Pierrynowski and Morrison, 1985). Another drawback to this method is

that the predictions are hard to validate, since invasive techniques such as inserting force transducers are not applicable in a human analysis. Regardless of the shortcomings, static optimization remains a frequently used tool in the determination of muscle forces.

In summary although inverse-dynamics is a valuable tool, it is limited in several respects. First, the determination of muscle force distribution from joint torques remains difficult, and the only validation of such a distribution is correlation with EMG recordings. Secondly the results from inverse-dynamics are highly dependent on accurate determination of joint angles and the calculation of joint torques (Patriarco *et al.*, 1981), but kinematic measurements are not always able to discern subtle movements which might be critical (Pandy and Berme, 1987). Another limitation associated with this method is that it is not predictive in nature, that is, one is limited to studying motion which is actually produced by the subjects being monitored. Additional drawbacks associated with inverse-dynamics can be found in Hardt (1978).

### 2.3 Direct-Dynamics

In a forward or direct-dynamical analysis the joint torques are the inputs and the body motion is the output. Thus equation (2.1) is rewritten in the following form to emphasize this relationship

$$\ddot{\theta} = M^{-1}[T + V + G + E].$$

It is important to realize what produces these joint torques. Joint torques are the accumulation of internal body forces such as ligaments, joint constraints, and of course, muscle forces. Muscles are the actuator in this system. Thus the true input into the system is indeed neural input. This neural input drives the muscles, and then the torques are an accumulation of both the passive and active structures which stabilize the body and propel it forward. Therefore controls for each muscle are needed to drive the system and the “redundancy problem” is revisited. Some type of optimization technique must again be utilized (Yamaguchi, 1992; Davy and Audu, 1987; Hatze, 1976; He, 1988; Levine *et al.*, 1983).

Although optimization techniques must still be utilized in this forward analysis, the optimization techniques employed are typically *dynamic*, meaning muscle dynamics are incorporated into the model. Muscle dynamics and the equations of motion governing the body are necessarily coupled. If a certain motion, like gait, is to be simulated, then the cost function usually involves both a tracking error term and a term influencing the distribution of muscle force, like energy consumption (Davy and Audu, 1987). Once controls are achieved, then the system of differential equations for the body and the system of differential equations governing the dynamics of each muscle group can be integrated forward in time to obtain the motion trajectories. Thus in a sense a direct-dynamic analysis is self-validating in that the controls specified do indeed result in the observed motion.

In this research, we choose to use a direct-dynamic approach for several reasons. When using a forward analysis, the loading conditions needed for a stress analysis of bone, i.e., joint torques, joint bending moments, joint reaction forces and individual muscle forces can be instantaneously derived as the model progresses forward in time. Since any motion is possible in a forward analysis, we are capable of generating an infinite amount of data. In addition, abnormalities in muscle function can be incorporated into the model. Thus fatigue or improper innervation in the musculotendon complex can be studied and the effects of such conditions on the integrity of the skeletal system can be quantified. In essence, we believe that a forward analysis provides the means to study a broader scope of loading conditions.

## CHAPTER III

### MUSCULOTENDON COMPLEX

As stated before, muscle is the active force producing organ in the body. Any forward analysis of gait relying on neural input as the control must incorporate a fairly accurate model of muscle into the simulation. Thus a working understanding of the basic function of muscle is fundamental to this research. Before describing a muscle model appropriate for gait simulation, some of the basic properties of the musculotendon complex should be discussed. For a more detailed description of muscle properties the reader is referred to McMahon's book, "*Muscles, Reflexes, and Locomotion*," or Zajac's Review, "*Muscle and Tendon: Properties, Model, Scaling, and Application to Biomechanics and Motor Control*."

#### 3.1 Architecture of Musculotendon

Muscles are connected to the bone through connective tissues called tendons and can be oriented to the tendon in a parallel or oblique fashion. These muscle types are referred to as parallel or pennate muscles respectively. See Figure 3.1 for the configuration of pennate muscles. All muscles in this study are treated as pennate muscles where  $\alpha$ , the pennation angle, quantifies the pennation for each muscle group. Although pennation angle varies depending on the state of contraction, the volume of muscle remains constant, a fact confirmed by Swammerdam in the 1660's (McMahon, 1984). The proximal attachment of the musculotendon unit to the bone is called the origin while the distal attachment is called the insertion. The length of the musculotendon which is dependent upon body configuration is defined as the length along the bones from origin to insertion.

The organization of muscle can be studied at various levels. Muscle generally refers to a bundle of muscle fibers which act in parallel. A single muscle fiber has a banded appearance. These bands divide the fiber into a series of sarcomeres, the smallest functional unit of a muscle (McMahon, 1984). This striated appearance is the result of the different refractive properties of the *A* and *I* bands in the sarcomeres (see Figure 3.2). At a microscopic level the sarcomeres are seen

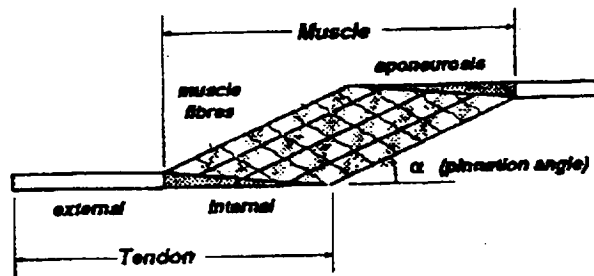


Figure 3.1: Geometry of Pennated Muscle. When muscles contract, they maintain a constant volume, and become more pennated. [Yamaguchi]

to be a collection of Myosin and F-actin myofilaments, referred to as thick and thin filament respectively. This microscopic architecture will be relevant when a theoretical explanation of force generation is described.

All levels of muscle structure down to the sarcomeres behave in a homogeneous fashion. Because of this homogeneity, each level can be viewed functionally as a scaled version of another level. Each sarcomere has the same relaxed length, and so the length of the muscle unit,  $L^m$ , is a measure of how many sarcomeres constitute one muscle fiber. Since each sarcomere produces the same amount of force  $F_s$  under similar circumstances and muscle fibers act in parallel, total muscle force  $F^m$  should be a scaled version of  $F_s$ . The scale factor between the sarcomere and the muscle unit is generally proportional to the mean cross-sectional area of that muscle unit, defined as weight in grams divided by length in centimeters (Zajac, 1989).

## 3.2 Functional Properties of the Musculotendon

### 3.2.1 Force-Length Properties of Muscle

Muscle force is easily measured at various lengths under isometric conditions to produce force-length relationships. The curve produced when muscle is not stimulated is referred to as the *passive force-length* curve,  $f_p(L^m)$ . When muscle is fully activated, the curve that results is called the tetanized curve and must



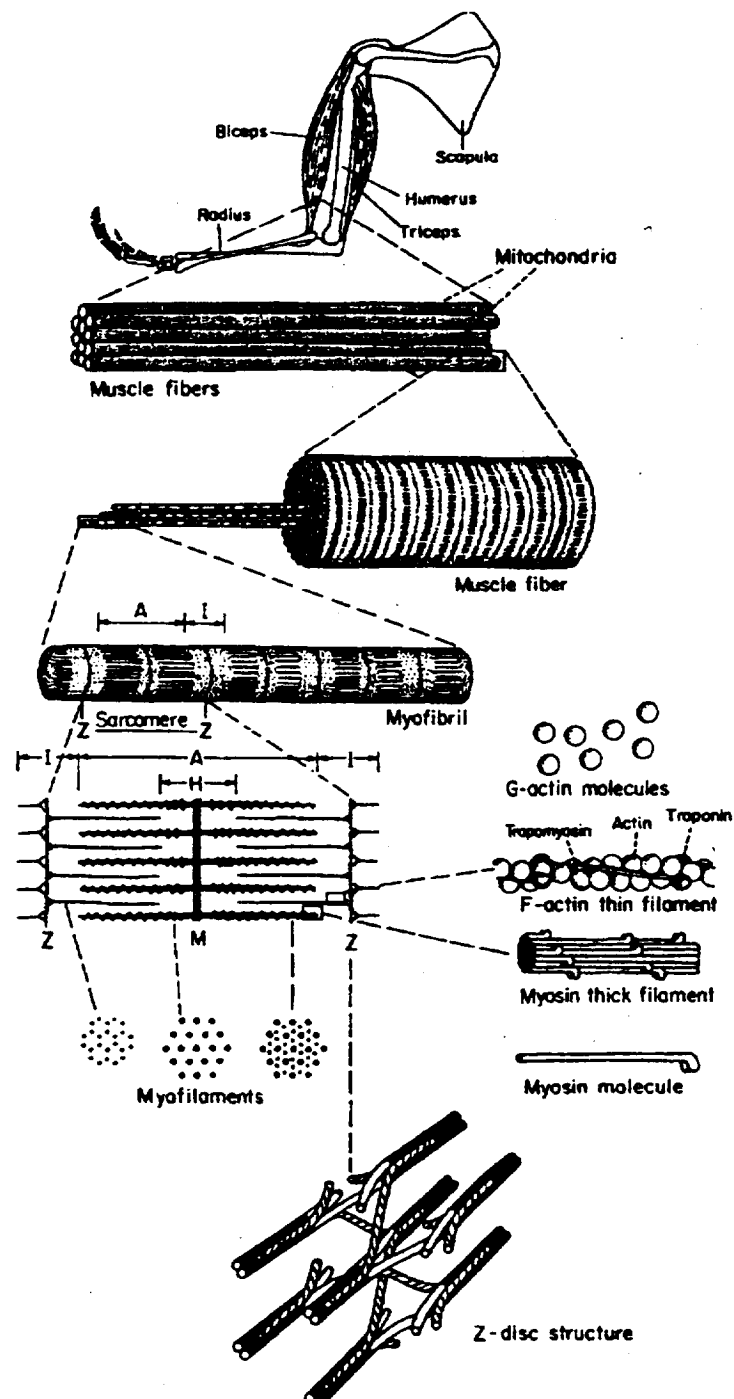


Figure 3.2: Organization of striated muscle. [McMahon]

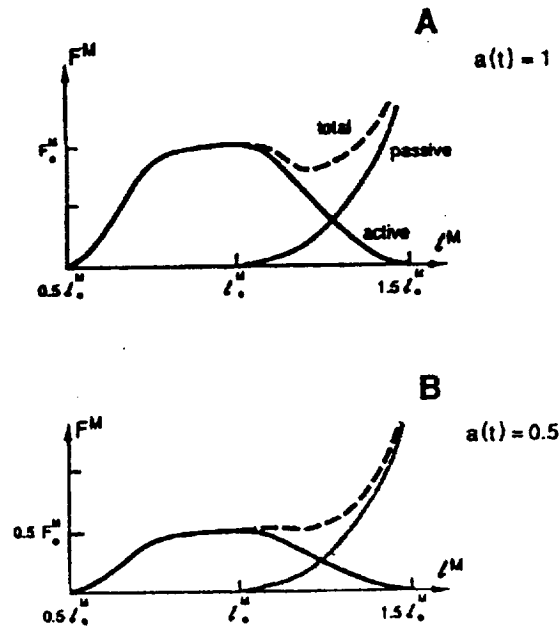


Figure 3.3: Isometric Force-Length Relation for Muscle: (A) Full activation, (B) Active force scales with activation but passive force is unaffected. [Zajac]

be the result of both passive and active contributions. The difference in these two curves is referred to as the *active force-length* relation,  $f_l(L^m)$ . The length at which the maximum active muscle force,  $F_o$ , is developed is called the optimal muscle length,  $L_o$ . See Figure 3.3 for the qualitative nature of these curves. At less than full activation, the *force-length* dependence is obtained by scaling the fully activated  $f_l$  curve (Winter, 1987; Zajac, 1989). The reason for the passive behavior is easily seen as just a consequence of the elastic material properties of muscle and is independent of activation.

A theoretical explanation for the active  $f_l$  relation is called the Sliding Filament Theory. This model was developed simultaneously by H. Huxley and A. Huxley (no relation) in the 1950's (McMahon, 1984), and is based on the microscopic nature of muscle (refer to Figure 3.2). It was proposed that during contraction the thick and thin filaments in sarcomeres slide past each other. Force is generated in the crossbridges that occur between actin and myosin during the overlap of

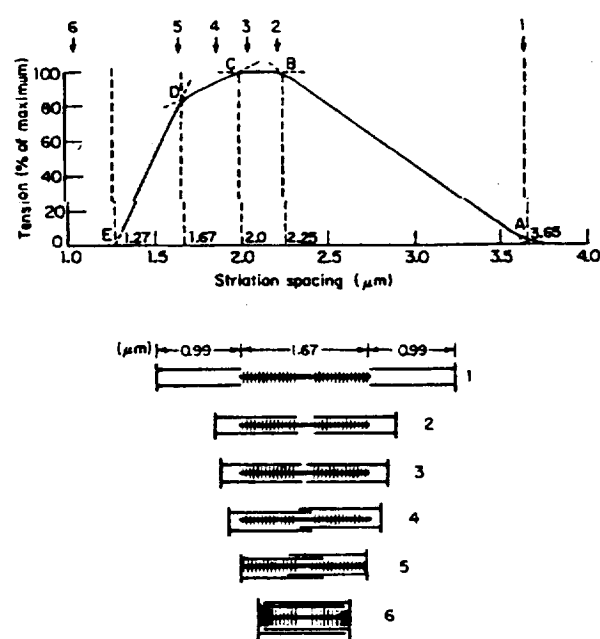


Figure 3.4: Active Tension-Length Curve for Muscles. [McMahon]

these filaments. Crossbridges can only occur in the presence of  $\text{Ca}^+$ . The calcium concentration is a byproduct of the activation level which explains why the  $f_l$  relation is scaled by activation. These crossbridges occur, rotate to move the filaments closer and then detach (McMahon, 1984). A. Huxley later proposed a mathematical model of the Sliding Filament Theory based on the probability of a crossbridge occurring. This theory properly explained the  $f_l$  curve (see Figure 3.4) and why force is only generated in a nominal region,  $.5L_o \leq L^m \leq 1.5L_o$  (Gordon *et al.*, 1966). This model has also been shown to predict many of the other features of muscle, for instance the *force-velocity* relation.

### 3.2.2 Force-Velocity Properties of Muscle

Active muscle force is also dependent on muscle velocity. When a muscle actively shortens (concentric contraction), it produces less force than it would under isometric conditions. A.V. Hill (1938) was the first to quantify this result with an

empirical hyperbolic relationship,

$$(F^m + a)(v^m + b) = (F_o + a)b. \quad (3.1)$$

So maximal active force is achieved when the velocity of the muscle,  $v^m$ , is zero, and the velocity (when  $L^m = L_o$ ) at which active force is zero is called maximum speed of shortening,  $v_o$ . Maximum speed of shortening is the limit to how fast a single unloaded crossbridge in the sacromere of a specific muscles can shorten (McMahon, 1984). The quickness of a crossbridge shortening determines whether muscles are classified as fast or slow.

In contrast to shortening, when a muscle is actively lengthening it is able to deliver forces above isometric forces. This relationship is not an extension of Hill's equation to the negative region, as might be expected. In fact, Katz discovered in 1939 that the slope of the *force-velocity* relation when muscle lengthens is six times steeper for slow-lengthening than for slow-shortening. He also showed that there is a threshold which limits the amount of tension muscle can withstand. This threshold is approximately  $1.8F_o$ . At tensions beyond this, the muscle is known to "give," a phenomena know as yielding (McMahon, 1984). A representation of the normalized *force-velocity* relation is depicted in Figure 3.5. This curve is also thought to scale with activation (Zajac, 1989).

It is clear now that active force generation is dependent on three factors: length of the muscle, velocity of the muscle and the activation level. There is evidence to suggest that total active force generation is best described by a *force-length-velocity* relationship which is usually quantified as the product of the *force-length* and *force-velocity* curves (Zajac, 1989; Winter, 1987). Therefore it is convenient to visualize force generation as a surface in three dimension, where each activation level determines a new surface (see Figure 3.6).

### 3.2.3 Force-Length Properties of Tendon

The tendon is composed of material both internal and external to the muscle (see Figure 3.1). The most relevant property of tendon with respect to gait studies is described by the *stress-strain* relationship depicted in Figure 3.7. This curve will be used in a later section to derive a generic *force-length* curve for tendon.

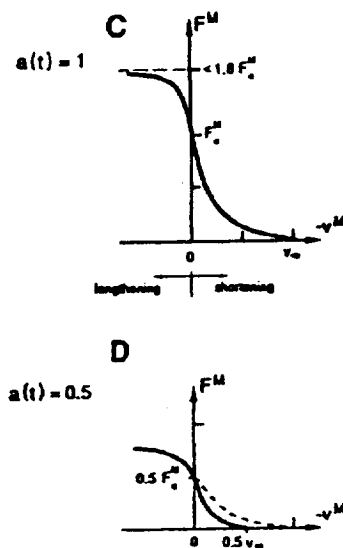


Figure 3.5: Force-Velocity Relation for Muscles (C) Full activation when  $L^m = L_o^m$ . (D) The *force-velocity* curve is also thought to scale with activation. [Zajac]

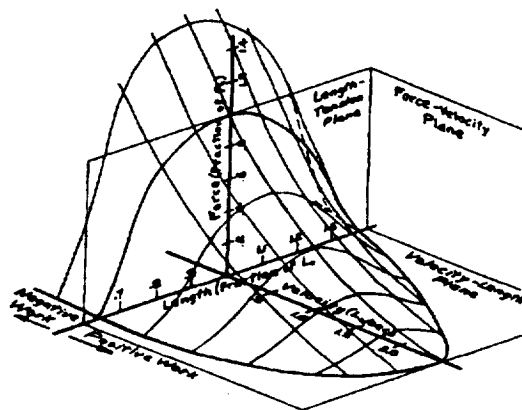


Figure 3.6: Three-dimensional surface plot showing the dependence of active force generation on both length and velocity of muscle. [Winter]

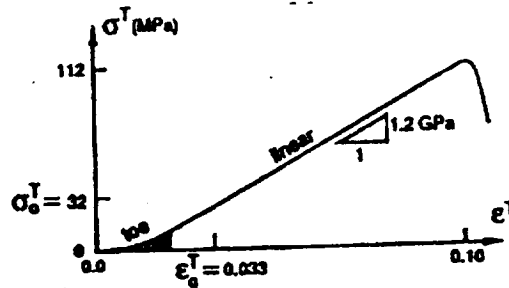


Figure 3.7: .  
Nominal Stress-Strain Curve for Tendons. [Zajac]

It is common to assume that the *stress-strain* property of tendon is homogeneous throughout internal and external portions. The tendon tangent of modulus of elasticity increases with strain in the “toe” region ( $\epsilon^t \leq .02$ ) and then becomes linear at higher strains until the tendon fails. Tendon failure occurs around 10% strain and 100 MPa (Zajac, 1989). The relevance of the interaction of tendon and muscle will be described in the next section.

## CHAPTER IV

### MUSCULOTENDON DYNAMIC MODEL

#### 4.1 Introduction

There are a couple of reasons why the muscle and tendon should be grouped together and treated as the musculotendon unit in gait analysis. Tendon and muscle act in series and when the tendon stretches an amount approaching  $L^m$ , the *force-length* characteristics of the grouped actuator differ significantly from the muscle alone. Thus it is important to treat the muscle and tendon as a musculotendon complex especially when the ratio  $L_t^*/L_o$  is large, as is the case with muscles around the ankle and knee (Zajac, 1989; Hoy *et al.*, 1990). Another reason they should be regarded as one unit is because they function together with the dynamics of the body. In fact, the muscle, tendon and body segments constitute a coupled, multiple-input multiple-output feedback system (Zajac, 1989). Figure 4.1 describes the interaction between these three units.

As seen from the figure, dynamics of the musculotendon complex can be viewed as two processes acting in series. Neural input drives the activation dynamics and outputs the muscle activation which is an internal state quantifying the ability of the cross-bridge structure of muscle to generate active force. Then muscle activation as well the length and velocity of the musculotendon are inputs into the musculotendon contraction dynamics, the process which outputs muscle force. These muscle forces then drive the body dynamics which effects the length and velocity of the musculotendon complex. Thus the dynamics of the whole system are highly coupled.

#### 4.2 Musculotendon Contraction Dynamics

##### 4.2.1 Scaling and Curves

When including several muscles in a model, it is advantageous to develop curves describing the attributes of a generic muscle. This model can then be scaled with appropriate parameters to reflect the dynamics of a particular muscle. In doing so, only four general curves need be specified: force-length function for passive

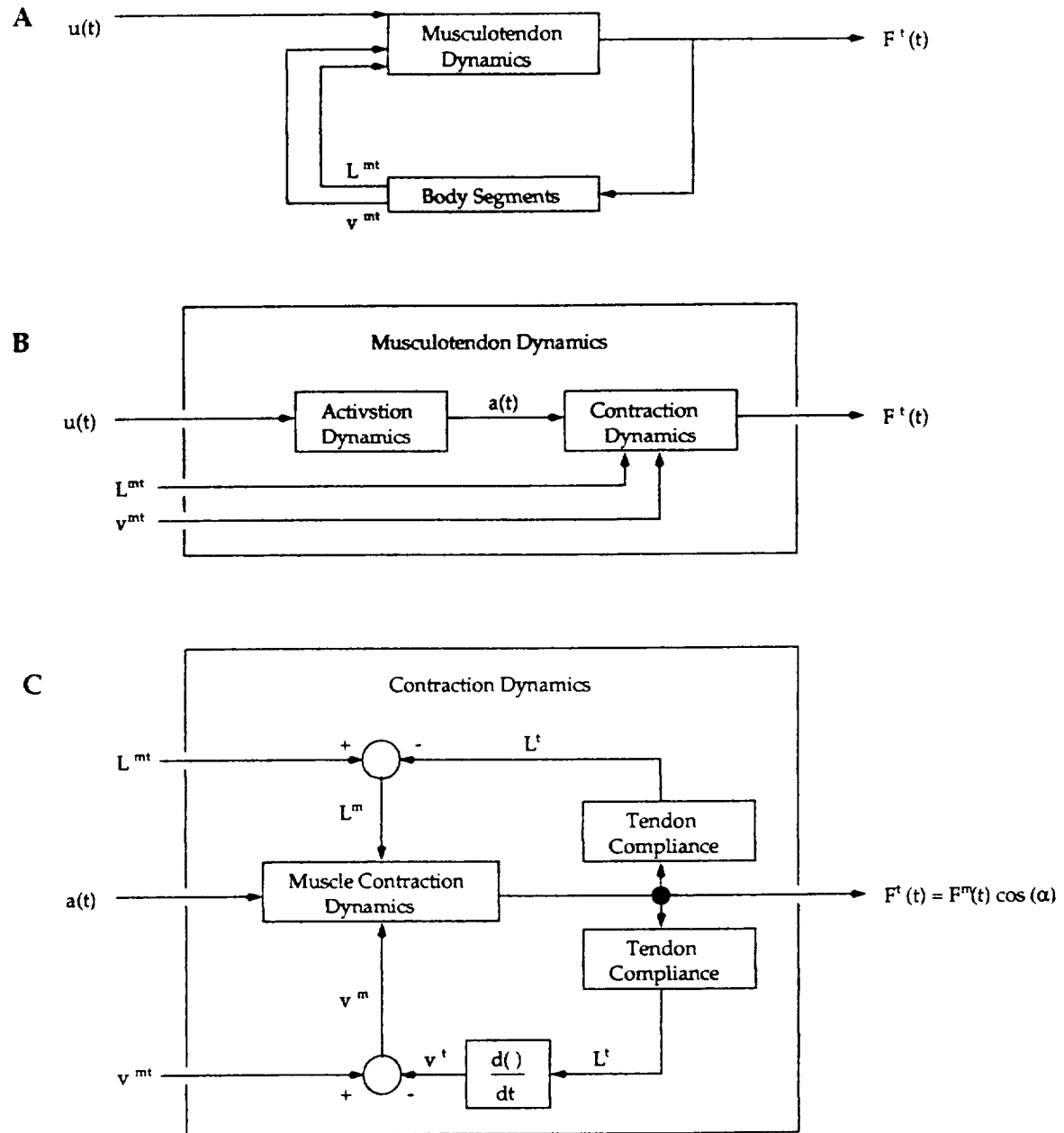


Figure 4.1: Block Diagram of the Coupled Dynamical Systems (A) Musculotendon actuators work with the body segments to produce the forces that propel the body. (B) Dynamics of the actuator consists of two uncoupled parts: activation dynamics and contraction dynamics. (C) Musculotendon contraction dynamics represent the interaction between muscle contraction dynamics and tendon compliance.



muscles, force-length function of active muscle, force-velocity function for active muscle and the force-length relation for tendons.

Scale parameters needed for each musculotendon group:

1. Maximal isometric active muscle force:  $F_o$ ,
2. Optimal muscle length:  $L_o$ ,
3. Pennation angle when  $L^m = L_o$ :  $\alpha_o$ ,
4. Tendon slack length:  $L_s^t$ .

All forces will be scaled by  $F_o$  and all lengths will be scaled by  $L_o$ . Maximum speed of shortening will be defined as,  $v_o \equiv L_o/\tau_c$ . This quantity is used to render the muscle specific *force-velocity* relation. This quantity  $\tau_c$  scales time and is known to vary for fast and slow muscles; however,  $\tau_c = .1s$  is standard value used for all muscles types (Zajac, 1989). Note then that  $v_o$  is not a new scale parameter in our model.

#### *Force-Length Relation for Passive Muscles ( $f_p(\tilde{l}^m)$ )*

This function represents the spring like behavior that muscles exhibit when activation is zero. A natural cubic spline which was fitted to data reported on Scott Delp's website ([www.kin.ucalgary.ca/isb/data/delp/delp\\_mus](http://www.kin.ucalgary.ca/isb/data/delp/delp_mus)) is utilized in this model. Figure 4.2 illustrates the spline as well as the reported data. The source of this data is well referenced (Delp and Loan, 1995; Delp *et al.*, 1990; Delp, 1990; Zajac, 1989).

#### *Force-Length Relation for Active Muscles ( $f_l(\tilde{L}^m)$ )*

This function represents the isometric force development in muscles when activation is 1, i.e., full activation. Note that force is only developed when  $\tilde{L}^m$  is in the nominal range:  $.5 \leq \tilde{L}^m \leq 1.5$ , as the "Sliding Filament Theory" suggests. Again a natural cubic spline was used which was fitted to data reported by Delp (Delp *et al.*, 1990). Figure 4.3 details the correspondence between the data and the splines.

#### *Force-Velocity Relation for Muscle ( $f_v^{-1}(\tilde{v}^m)$ )*

This curve accounts for the fact that muscle cannot change its length instantaneously and that the contractile component is damped by a visous effect. Although

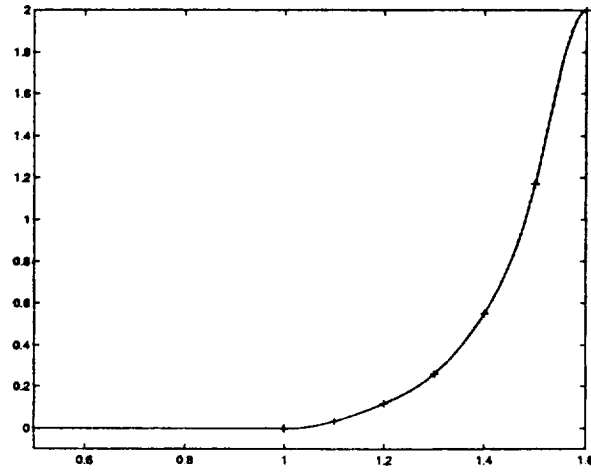


Figure 4.2: Isometric Passive Force-Length for Muscles:  $\tilde{F}^m$  vs.  $\tilde{l}^m$

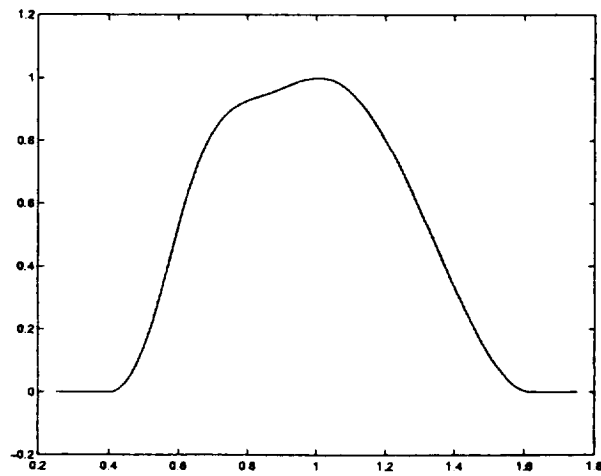


Figure 4.3: Isometric Active Force-Length for Muscles:  $\tilde{F}^m$  vs.  $\tilde{l}^m$

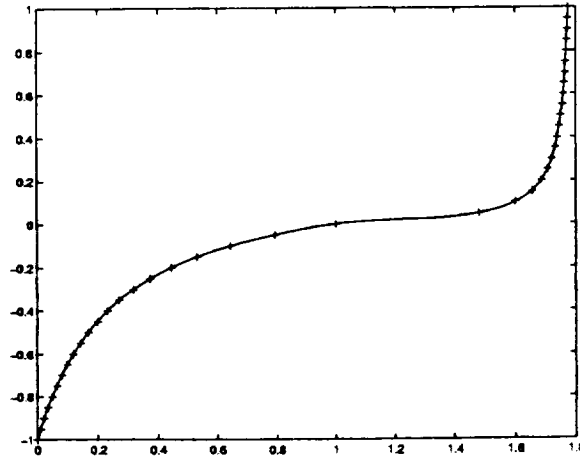


Figure 4.4: Inverse Force-Velocity Relation for Muscles:  $\tilde{v}^m$  vs.  $\tilde{F}$

Hill's equation (3.1) is believed to model force development when a muscle is shortening, we choose instead to use a natural cubic spline which was fit to data collected while the muscle lengthened and shortened (Delp *et al.*, 1990). Due to the way the curve is utilized in the formulation of the dynamics, it is convenient to express this relation in terms of the inverse  $f_v^{-1}(\tilde{F})$ . The curve is depicted along with the data in Figure 4.4. The output of the inverse will be normalized with respect to  $v_o$ , the maximum speed of shortening. In particular where  $\tilde{F}$  denotes a normalized active muscle force,

$$\tilde{v}^m = v^m/v_o = f_v^{-1}(\tilde{F}).$$

#### *Force-Length Relation for Tendon*

A generic force-length relationship for tendon is derived by a method discussed by Zajac. Define tendon strain by  $\varepsilon^t = (L^t - L_s^t)/L_s^t$  and normalized tendon force by  $\tilde{F}^t = F^t/F_o$ . Zajac assumes a generic *force-strain curve* ( $\tilde{F}^t$  vs.  $\varepsilon^t$ ) based on the following two assumptions (see Figure 4.5):

1. A nominal *stress-strain* curve can be formulated that represents all tendon (refer to Figure 3.7).

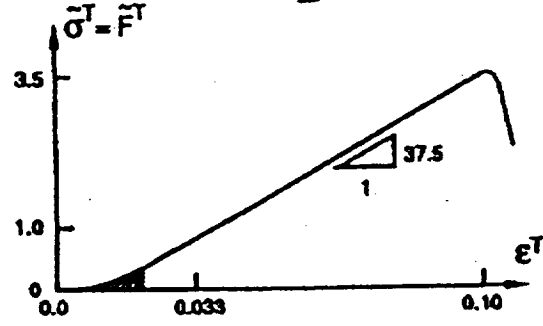


Figure 4.5: Generic Force-Strain Relation for Tendons:  $\bar{\sigma}^t = \bar{F}^t$  vs.  $\epsilon^t$  [Zajac]

2. The strain in a tendon when force in the tendon equals the maximal isometric muscle force is independent of the musculotendon unit. We refer to this strain as  $\epsilon_o^t$ , and once this value is specified it determines a nominal value of stress,  $\sigma_o^t$ . Although the value of each of these quantities is disputed, we will take  $\epsilon_o^t = 0.033$  and  $\sigma_o^t = 32MPa$  (Zajac, 1989).

Once these assumptions are agreed upon, the *force-strain* relation is achieved by scaling stress by  $\sigma_o^t$  in the *stress-strain* curve and noting that

$$\frac{\sigma^t}{\sigma_o^t} = \frac{F^t/A}{F_o/A} = \bar{F}^t,$$

where  $A$  is the mean cross-sectional area of the tendon. Thus by scaling this generic *force-strain* relationship by  $F_o$  and  $L_o^t$ , a *force-length* function is found for the tendon.

We use the following function to describe the normalized *force-strain* relationship

$$F_t(\epsilon^t) = \begin{cases} .10377(e^{91\epsilon^t} - 1) & 0 \leq \epsilon^t < .01516 \\ 37.526\epsilon^t - .26029 & .01516 \leq \epsilon^t < .1 \end{cases} \quad (4.1)$$

Figure 4.6 shows the correspondence between this function and data reported by Delp. If the strain in tendon reaches values beyond .1, the tendon is known to rupture (Zajac, 1989). Since such an extreme value of strain should not occur

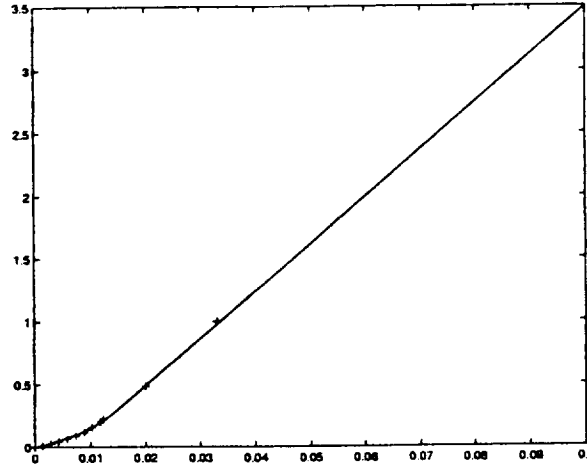


Figure 4.6: Force-Strain Relation for Tendons:  $\tilde{F}^t$  vs.  $\varepsilon^t = \frac{L^t - L_s^t}{L_s^t}$

during normal locomotion, this part of the curve need not be included in our analysis.

Also derived from equation (4.1) is absolute tendon stiffness which defined by,  $K^t(F^t) \equiv dF^t/dL^t$ . Observe that

$$\begin{aligned}
 K^t(F^t) &= \frac{dF^t}{d\tilde{F}^t} \cdot \frac{d\tilde{F}^t}{d\varepsilon^t} \cdot \frac{d\varepsilon^t}{dL^t} \\
 &= \frac{F_0}{L_s^t} \cdot \frac{d\tilde{F}^t}{d\varepsilon^t} \\
 &= \begin{cases} \left(\frac{F_0}{L_s^t}\right) 91(\tilde{F}^t + .10377) & 0 \leq \tilde{F}^t \leq .3086 \\ \left(\frac{F_0}{L_s^t}\right) 37.526 & \tilde{F}^t \geq .3086 \end{cases} . \quad (4.2)
 \end{aligned}$$

#### 4.2.2 Derivation of Contraction Dynamics of Musculotendon Unit

The dynamics for the model of the musculotendon unit depicted in Figure 4.7 can now be derived by utilizing the curves defined in the previous section. The model used is referred to as a Hill-type model and represents the properties of the musculotendon as idealized mechanical objects. This model has been shown

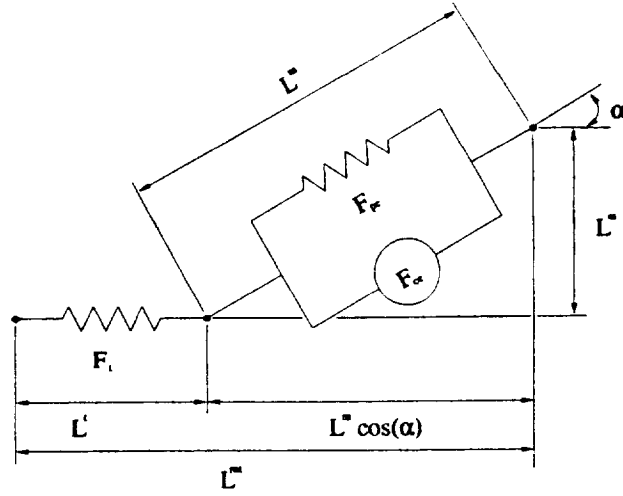


Figure 4.7: Hill Type Model of the Musculotendon.

to incorporate enough complexity while remaining computationally practical, thus qualifying itself as a good model for use in gait simulations (Audu, 1985). Muscle mass is assumed to be negligible in this formulation even though there are some stability issues which arise if muscle mass is absent in the dynamics (He, 1988).

The length of the musculotendon  $L^{mt}$  is defined to be the distance from origin to insertion, as stated previously. Note that this quantity is a function of the segmental orientations. From Figure 4.7, it is clear  $L^{mt}$  also satisfies the following equation:

$$L^{mt} = L^t + L^m \cos \alpha. \quad (4.3)$$

Muscle is known to maintain a constant volume. In two dimensions, this implies  $L^w$  is constant, and so

$$L^w = L^m \sin \alpha = L_o \sin \alpha_o. \quad (4.4)$$

$F_{CE}$  is the force developed by the contractile element (CE), and  $F_{PE}$  is the force developed by the passive element (PE). Thus the force in the muscle is given by

$$F^m = F_{CE} + F_{PE} = F_o a(t) f_l(\tilde{L}^m) f_v(\tilde{v}^m) + F_o f_p(\tilde{L}^m). \quad (4.5)$$

Due to a force balance,

$$F_t = F^m \cos \alpha. \quad (4.6)$$

The dynamics for the musculotendon are expressed by

$$\frac{dF^t}{dt} = \frac{dF^t}{dL^t} \cdot \frac{dL^t}{dt} = K^t(F^t) \dot{L}^t. \quad (4.7)$$

Now an expression for  $\dot{L}^t$  can be formulated by differentiating equation (4.3),

$$\dot{L}^t = \dot{L}^{mt} - (\dot{L}^m \cos \alpha - L^m \sin \alpha \dot{\alpha}). \quad (4.8)$$

Since  $L^w$  is constant, differentiation of equation (4.4) yields an expression for  $\dot{\alpha}$ ,

$$0 = \dot{L}^m \sin \alpha + L^m \cos \alpha \dot{\alpha} \quad \Rightarrow \quad \dot{\alpha} = -\frac{\dot{L}^m}{L^m} \tan \alpha \quad (4.9)$$

Substitution of  $\dot{\alpha}$  into equation (4.8) gives

$$\begin{aligned} \dot{L}^t &= \dot{L}^{mt} - \dot{L}^m (\cos \alpha + \sin \alpha \tan \alpha) \\ &= \dot{L}^{mt} - \frac{\dot{L}^m}{\cos \alpha}. \end{aligned} \quad (4.10)$$

Since  $v^m = \dot{L}^m$ , equations (4.5) and (4.6) can be used to solve for  $\dot{L}^m$ . In particular we have

$$F^t = F^m \cos \alpha = (F_o a(t) f_l(\tilde{L}^m) f_v(\tilde{v}^m) + F_o f_p(\tilde{L}^m)) \cos \alpha \quad (4.11)$$

$$\Rightarrow \quad \tilde{v}^m = \frac{v^m}{v_o} = f_v^{-1} \left( \frac{(F^t / \cos \alpha) - F_o f_p(\tilde{L}^m)}{F_o a(t) f_l(\tilde{L}^m)} \right), \quad (4.12)$$

and so

$$\dot{L}^m = v^m = v_o f_v^{-1} \left( \frac{(F^t / \cos \alpha) - F_o f_p(\tilde{L}^m)}{F_o a(t) f_l(\tilde{L}^m)} \right). \quad (4.13)$$

Thus the differential equation describing the contraction dynamics of the musculotendon is

$$\frac{dF^t}{dt} = \frac{F_0}{L_s^t} K^t(\tilde{F}^t) \left[ \dot{L}^{mt} - \frac{v_o}{\cos \alpha} f_v^{-1} \left( \frac{(F^t / \cos \alpha) - F_0 f_p(\tilde{L}^m)}{F_0 a(t) f_l(\tilde{L}^m)} \right) \right] \quad (4.14)$$

where

$$v_o = 10L_0,$$

$$\tilde{L}^m = \frac{L^m}{L_0} = \frac{\sqrt{(L^{mt} - L^t)^2 + (L^w)^2}}{L_0},$$

$$L^t = \begin{cases} L_s^t \left( 1 + \frac{\ln\left(\frac{\tilde{F}^t}{.10377} + 1\right)}{91} \right) & 0 \leq \tilde{F}^t \leq .3086 \\ L_s^t \left( 1 + \frac{\tilde{F}^t + .26029}{37.526} \right) & .3086 \leq \tilde{F}^t \end{cases},$$

$$\cos \alpha = \frac{L^{mt} - L^t}{L^m},$$

$$\tilde{F}^t = \frac{F^t}{F_0}.$$

### 4.3 Activation Dynamics

In this model of the musculotendon complex, neural excitement,  $u(t)$ , is regarded as a control variable which varies between 0 and 1. Neural excitement is related to contraction dynamics by activation,  $a(t)$ , which scales the *active force-length* and *force-velocity* curves. Activation varies between 0 and 1, but due to the formulation of the contraction dynamics it is necessary to specify a minimum activation which is not zero, i.e.,  $0 < a_{min} \leq a(t) \leq 1$ . This process through which neural input is transformed into activation is called activation dynamics and is known to be mediated through a calcium diffusion process (McMahon, 1984). Although there is some evidence to suggest that activation dynamics are not independent of contraction dynamics (Zajac, 1989), we adopt the common assumption of independence.



Both quantities,  $u(t)$  and  $a(t)$ , can be related to experimental data, i.e. EMG recordings. In this case,  $u(t)$  is related to rectified EMG while  $a(t)$  is related to filtered, rectified EMG (Zajac, 1989). This relationship between  $u(t)$  and  $a(t)$  can be represented by the following bilinear form

$$\frac{da(t)}{dt} + \left[ \frac{1}{\tau_{act}} \cdot (\beta + (1 - \beta)u(t)) \right] \cdot a(t) = \frac{1}{\tau_{act}} \cdot u(t) \quad (4.15)$$

where

$$0 < \beta < 1.$$

Note that activation is fastest with time constant  $\tau_{act}$  when  $u(t) = 1$  and slowest with time constant  $\tau_{act}/\beta$  when  $u(t) = 0$ . We took  $\tau_{act} = .012s$  (Zajac, 1989), and  $\beta = .1$  (Pandy *et al.*, 1990).

As will be discussed, the controls for the muscles incorporated in this model were adapted from Yamaguchi's dissertation. To simplify the optimization technique utilized in creating these controls, he assumed  $u(t)$  to be piece-wise constant. With such an assumption, it is possible to find a closed form solution to the differential equation (4.15). In particular, assume

$$u(t) = u_o \quad t_i \leq t < t_f$$

Then,

$$a(t) = u_o + (a(t_i^-) - u_o)e^{-\frac{1}{.012}(.1 + .9u_o)(t-t_o)} \quad t_i \leq t < t_f \quad (4.16)$$

where

$$a(t_i^-) = \lim_{t \rightarrow t_i^-} a(t).$$

This simplification was useful in the simulation of our model since the number of differential equations to be solved is large and thus represents additional computer time. Figure 4.8 shows how the activation dynamics responds to a step input. Thus activation lags behind neural input with activation occurring at a more rapid rate than deactivation.

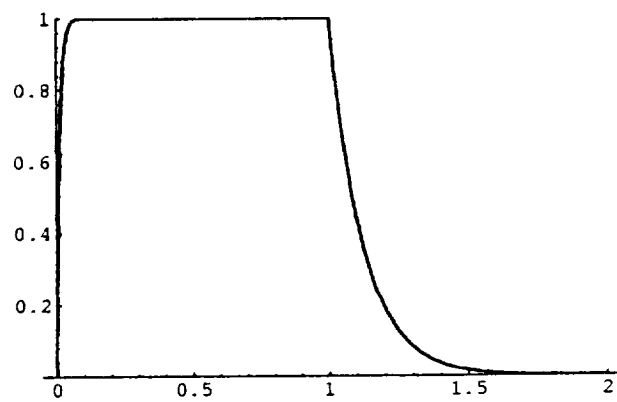


Figure 4.8: Activation Dynamics:  $a(t)$  vs.  $t$ . This graph represents the response of the activation dynamics to a step input of neural activation, i.e.,  $u(t) = \chi_{[0,1]}$ .

## CHAPTER V

### THE MUSCULOSKELETAL MODEL

#### 5.1 Introduction

In order to generate the loading conditions relevant during gait, it was necessary to develop a model driven by musculotendon actuators which could simulate normal and pathological gait. Although many gait models have been built, few included the complexity which is needed for realistic dynamic simulations. It was decided that a model developed by Gary Yamaguchi (1989) represented a good initial choice. With this model, it could be determined if the additional loading conditions provided by accurate descriptions of muscle forces would be beneficial in characterizing stress development in bones. Thus the following description of the musculoskeletal model is adapted from the dissertation work of Yamaguchi.

Before a discussing the actual model, it is important to realize the original goal of the research pursued by Yamaguchi. In his study the feasibility of using functional neuromuscular stimulation (*FNS*) to enable a paraplegic to walk with normal appearance and speed was questioned. *FNS* is a process where electrical currents are artificially applied to nerve and muscle tissue in order to stimulate muscles. In Yamaguchi own words, "The goal of the study was to examine whether minimal sets of muscles could be used in order to generate approximately normal gait trajectories without requiring either high levels of force or unduly precise control of muscle activation" (Yamaguchi, 1990, pg v). In order to study the feasibility of *FNS*, it was necessary for Yamaguchi to develop a model capable of reproducing most of the known "determinants" of gait as classified by Saunders *et al.* in 1953 while maintaining a practical limitation on the degrees of freedom as dictated by the technology available at that time.

#### 5.2 Skeletal Model

The following is a brief synopsis of the model utilized in our research and the reader is referred to Yamaguchi's dissertation for more details. The model constrains seven rigid-body segments which represent the feet, shanks, thighs and

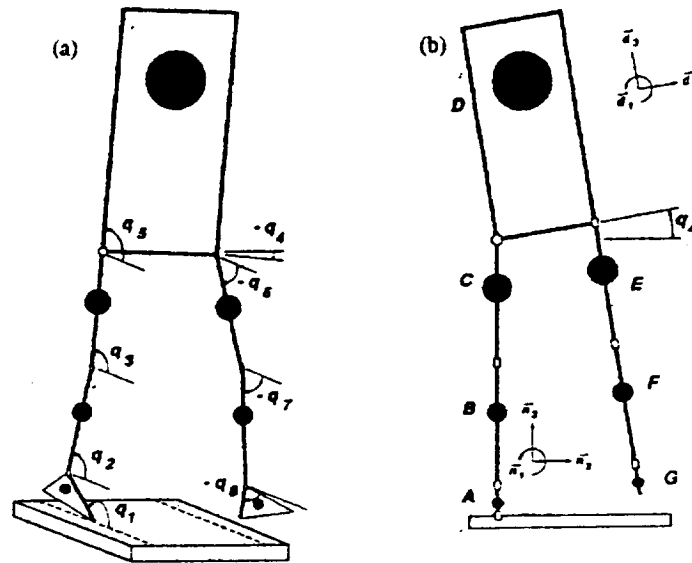


Figure 5.1: 3-D, 8 DOF Model Showing Segment Angle Definitions: (a) The stance hip has two DOF, while all other joints are revolute. (b) Front view showing pelvis list. Stance angles are specified with respect to the inertial frame,  $\vec{n}$ , while the swing angles are respect to the titled trunk reference frame,  $\vec{d}$ . [Yamaguchi]

trunk to 8 degrees of freedom. All joints are assumed to be revolute having one degree of freedom with the exception of the stance hip which has two degrees of freedom. This allows the hip to ab/adduct, a condition which reduces the degree of coupling between the trunk and the swing leg (Yamaguchi, 1989). Figure 5.1 shows the generalized coordinates which were used to describe the configuration of the body. Joint angles  $q_1$ ,  $q_2$ , and  $q_3$  are measured with respect to the horizontal or transverse plane and the rotation of these joints occur about an axes parallel to  $\vec{n}_2$ . Movement of the stance leg is confined to the sagittal plane, but due to the extra degree of freedom granted to the stance hip, the swing leg and trunk can also move in the frontal or coronal plane through pelvic list. Joint angle  $q_4$  tilts the trunk as well as the swing leg about an axis parallel to  $\vec{n}_1 = \vec{d}_1$ . Joint angles  $q_5$  through  $q_8$  are measured in the titled plane and these rotations occur about an axis which is parallel to  $\vec{d}_2$ .

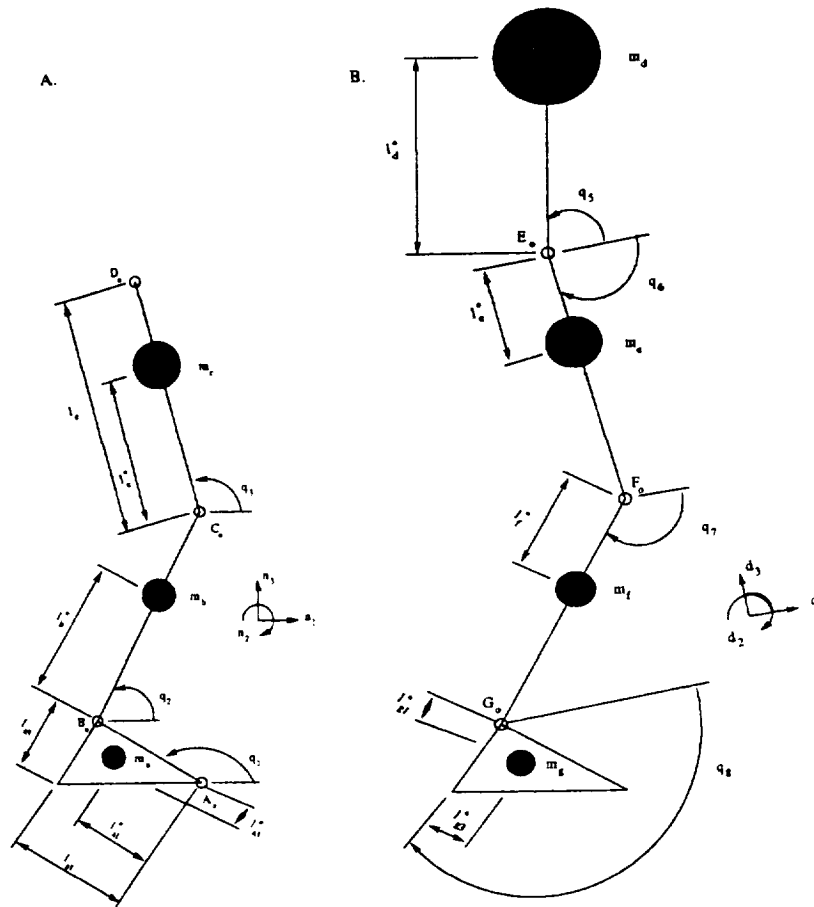


Figure 5.2: Definition for Inertial and Segmental Parameters: (a) Stance Leg (sagittal plane) (b) Swing Leg (titled plane).

This musculoskeletal model represents a normal male with mass totaling 76 kilograms. Figure 5.2 shows the definitions for the segmental dimensions and the inertial parameters used to specify this model. Segmental dimensions and inertial parameters are listed in Table 5.1 (Yamaguchi 1989).

A key element of the model is that only one-half (14%, approximately left-toe-off, to 62%, approximately left-foot-flat) of the gait cycle is simulated in this analysis. The complete gait cycle (see Figure 5.3) can be reconstructed under the assumption of bilateral symmetry. Bilateral symmetry is not always valid since many asymmetries in gait have been reported (Winter, 1979); however, the

Table 5.1: Segment dimensions and inertial parameters used in this model (see Figure 5.2). All starred items are given with respect to the segments' center of mass. (Yamaguchi 1989)

	lengths (m)	mass (kg)	principal moments of inertia (kg-m <sup>2</sup> )
foot	$l_{a1} = 0.175$ $l_{a3} = 0.118$ $l_{a1}^* = 0.100$ $l_{a3}^* = 0.0295$	$m_a = 1.10$	$I_{a1}^* = 0.002$ $I_{a2}^* = 0.008$ $I_{a3}^* = 0.009$
shank	$l_b = 0.435$ $l_b^* = 0.247$	$m_b = 3.75$	$I_{b1}^* = 0.019$ $I_{b2}^* = 0.065$ $I_{b3}^* = 0.065$
thigh	$l_c = 0.410$ $l_c^* = 0.227$	$m_c = 7.58$	$I_{c1}^* = 0.080$ $I_{c2}^* = 0.126$ $I_{c3}^* = 0.126$
trunk	$l_d = 0.172$ $l_d^* = 0.343$	$m_d = 51.22$	$I_{d1}^* = 0.764$ $I_{d2}^* = 3.407$ $I_{d3}^* = 3.297$
	$l_e = l_c$ $l_e^* = l_c - l_c^*$ $l_f = l_b$ $l_f^* = l_b - l_b^*$ $l_{g3} = l_{a3}$ $l_{g1}^* = l_{a3}^*$ $l_{g3}^* = l_{a1} - l_{a1}^*$	$m_e = m_c$ $m_f = m_b$ $m_g = m_a$       	$I_{e1,e2,e3}^* = I_{c1,c2,c3}^*$ $I_{f1,f2,f3}^* = I_{b1,b2,b3}^*$ $I_{g1}^* = I_{a3}^*$ $I_{g2}^* = I_{a2}^*$ $I_{g3}^* = I_{a1}^*$

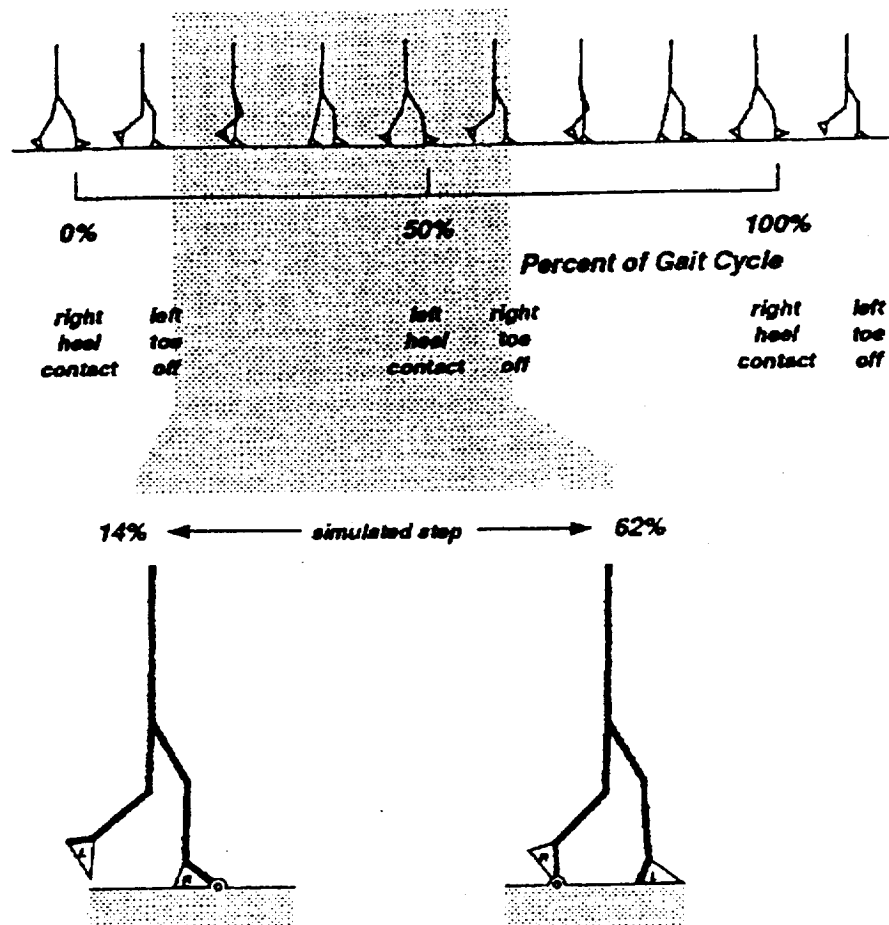


Figure 5.3: Simulated Gait Cycle With Respect to Total Gait Cycle. This model assumes bilateral symmetry to reproduce 96% of the cycle. [Yamaguchi]

advantages of this assumption warrant its inclusion. This assumption simplifies the modeling in that the stance leg is always the stance leg and the swing leg is always the swing leg. As a result, muscles in the swing and stance leg can vary according to the function of that leg in the simulation. With this assumption, it is also valid to have the stance toe constrained to the ground which eliminates one more degree of freedom. Thus this simplification requires less muscles to be modeled and less degrees of freedom.

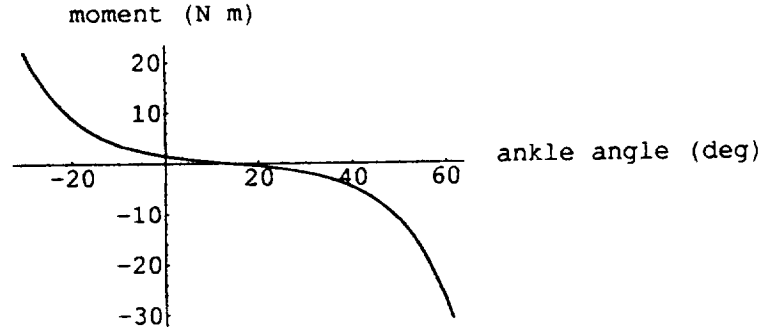


Figure 5.4: Passive Joint Moment for Ankle Joint. Positive angles and moments correspond to plantarflexion of the ankle.

### 5.3 Passive Constraints at the Joints

The range of each joint angle was limited to normal ranges through the use of ligamentous constraints. If the joint angle stays within a nominal range, then the effects of the passive structure are minimal, but when the nominal range is exceeded the passive torques grow exponentially. The general form of the passive moments is given by

$$M_{pass} = k_1 e^{-k_2(\theta-\theta_2)} - k_3 e^{-k_4(\theta_1-\theta)} - c\dot{\theta} \quad (5.1)$$

where  $\theta$  is the joint angle measured in radians,  $\dot{\theta}$  is the joint velocity measured in radian per second and  $M_{pass}$  is measured in Newton-meters. Note that  $\theta_2 < \theta < \theta_1$  represents a nominal range for that joint. The parameters  $k_j$ ,  $\theta_j$ , and  $c$  were taken from Davy and Audu (1985, 1987) and modified by Yamaguchi (1989). Included in this passive moment is a damping term,  $-c\dot{\theta}$ . This is vital to the model since a damping term was not included in the musculotendon model. See Table 5.3 for a list of the passive parameters and definitions of the joint angles in terms of the generalized coordinates. Figures 5.4 through 5.6 depict the passive joint torques under static conditions, i.e., neglecting the damping term.



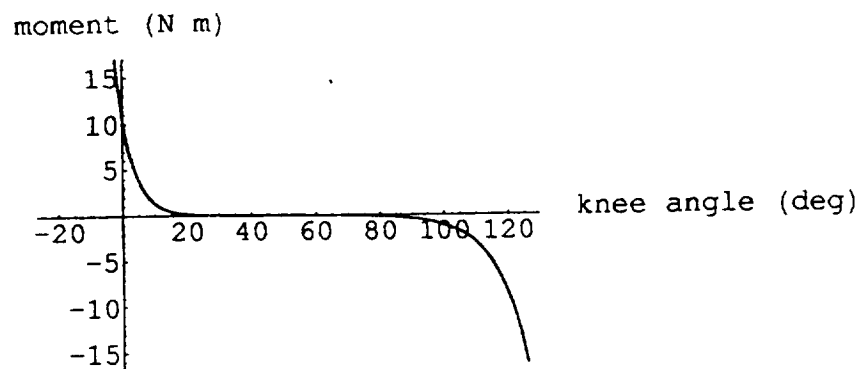


Figure 5.5: Passive Joint Moment for Knee Joint. Positive angles and moments correspond to flexion of the knee.

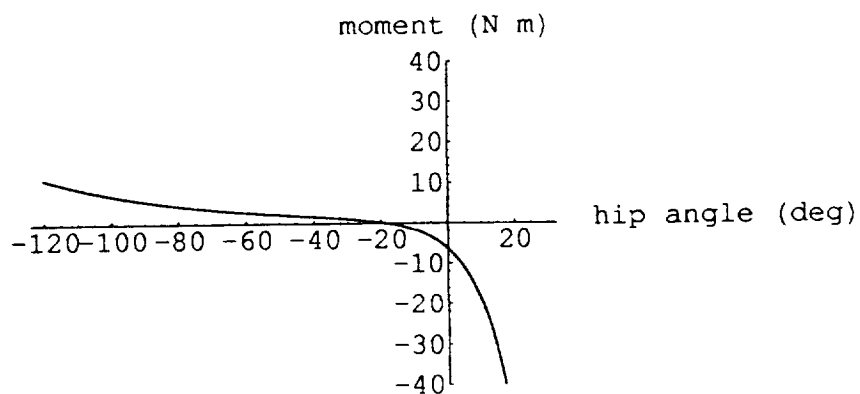


Figure 5.6: Passive Joint Moment for Hip Joint. Positive angles and moments correspond to extension of the hip.

Table 5.2: Coefficients for Passive Joint Moments

ankle $\theta_{stance} = q_1 - q_2 + .5934$ $\theta_{swing} = 2.1642 - (q_8 - q_7)$	$k_1 = 2.0$ $k_2 = 5.0$ $k_3 = 9.0$ $k_4 = 5.0$	$c_1 = 9.43$ $\theta_1 = 1.92$ (20° dorsiflexion) $\theta_2 = 1.047$ (30° plantarflexion)
knee $\theta_{stance} = q_2 - q_3$ $\theta_{swing} = q_6 - q_7$	$k_1 = 3.1$ $k_2 = 5.9$ $k_3 = 10.5$ $k_4 = 11.8$	$c_1 = 3.17$ $\theta_1 = 0.00$ (full extension) $\theta_2 = -1.92$ (110° flexion)
hip $\theta_{stance} = q_3 - q_5$ $\theta_{swing} = 3.14 - (q_5 + q_6)$	$k_1 = 2.6$ $k_2 = 5.8$ $k_3 = 8.7$ $k_4 = 1.3$	$c_1 = 1.09$ $\theta_1 = 1.92$ (110° flexion) $\theta_2 = 0.1744$ (10° flexion)

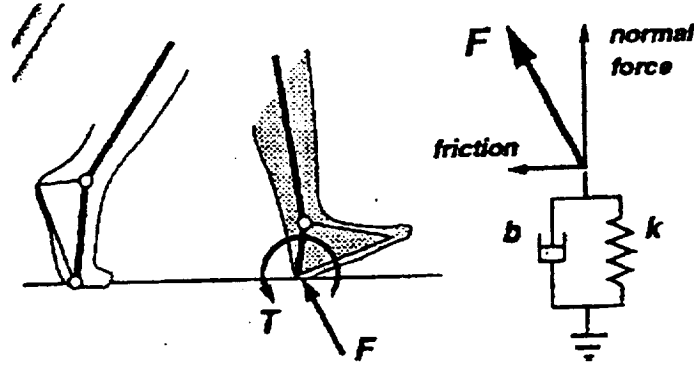


Figure 5.7: "Soft" Constraint on Swing Leg During Double Support [Yamaguchi]

#### 5.4 Soft Floor Constraints

Although the stance toe is constrained throughout the simulation, it was necessary to incorporate additional constraints in order to prevent the stance heel and swing foot from penetrating the "ground" and to eliminate excess sliding of the swing foot during double support. These additional constraints are considered to be "soft" (Hemami, 1975). The vertical ground reaction forces which acted on the heels of both the stance and swing leg were modeled as highly-damped, stiff linear springs

$$F_{normal} = \begin{cases} 0 & z_{heel} \geq 0 \\ -(1.5 \times 10^5)z_{heel} - (1 \times 10^3)\dot{z}_{heel} & z_{heel} < 0 \end{cases} \quad (5.2)$$

where  $z_{heel}$  is the height of the heel above the ground. On the swing heel an additional frictional force applied in a direction parallel to the ground in the sagittal plane is used to prevent excess sliding (see Figure 5.7). This force is proportional to the normal force applied to the swing heel,

$$F_{friction} = \begin{cases} 0 & z_{heel_{swing}} \geq 0 \\ -.5|F_{normal}(z_{heel_{swing}})| & z_{heel_{swing}} < 0 \end{cases} \quad (5.3)$$

Once flat-foot is achieved by the swing leg a counterclockwise torque is applied to prevent the foot from penetrating the ground. The torque is model as a damped,

torsional spring which resists plantarflexion of the foot. This torque is given by

$$T = \begin{cases} 0 & z_{heel_{swing}} > 0 \text{ or } \delta \geq 0 \\ -5696\delta - 38.19\dot{\delta} & z_{heel_{swing}} \leq 0 \text{ and } \delta < 0 \end{cases} \quad (5.4)$$

where  $\delta$  is the angle the bottom of the foot makes with the ground.

These “soft” constraints allow the same model to be used during the single and double support phases of gait. If the ground had been modeled as “hard” constraint, then one would lose a degree of freedom on the swing leg when the toe touches the ground. This would mean two models would be needed to simulate this phase of gait and a switch between the two systems would occur at heel strike.

## 5.5 Incorporating the Musculotendon Actuators

### 5.5.1 Minimal Set of Muscles

As stated earlier, one of the goals of Yamaguchi’s dissertation was to find a minimal muscle set needed to simulate normal gait. This minimal set of muscles (see Figure 5.8) as well as the controls for each musculotendon actuator was determined by a dynamic optimization technique which will be discussed later. This set was found to be in good qualitative agreement with record EMG activity during gait (Yamaguchi, 1989). We will use the same muscle sets as his program derived. As a result, ten musculotendon units are incorporated into our model, five on each leg (refer to Figure 5.8). On the stance leg, the relevant muscle groups are the Soleus, Gastrocnemius, Vasti, Gluteus Medius & Minimus, and the Iliopsoas. While the swing leg utilizes the Dorsiflexors, Hamstring, Vasti, Gluteus Medius and Minimus and the Iliopsoas. Thus seven different musculotendon groups need to be specified in this model. Table 5.3 shows the constituent muscles composing each musculotendon group, and Table 5.4 gives a list of the parameters which are used to distinguish the dynamics of each particular musculotendon unit.

### 5.5.2 Origins and Insertions

In order to incorporate these musculotendon into the dynamics, we must place the muscles geometrically on the body segment so that the length of the musculotendon,  $L^{mt}$  and the velocity of the musculotendon,  $v^{mt}$ , can be derived as a

Table 5.3: Musculotendon Groups and Their Constituent Muscles (Hoy *et al.*, 1989; Yamaguchi, 1989)

Musculotendon Groups	Constituent Muscles
Iliopsoas	Iliacus Psoas
Gluteus Medius & Minimus	Gluteus Medius Gluteus Minimus
Hamstring	Semitendinosus Semimembranosus Biceps Femoris, long head
Vasti	Vastus Lateralls Vastus Medialis Vastus Intermedius
Gastrocnemius	Gastrocnemius Laterails Gastrocnemius Medialis
Soleus	Soleus
Dorsiflexors	Tibialia Anterior Extensor Digitorum Longus Extensor Hallucia Longus Peroneus Tertius

Table 5.4: Parameters Defining the Musculotendon Actuators (Hoy *et al.*, 1989; Yamaguchi, 1989).

Musculotendon Actuator	Maximum Isometric Strength $F_o^m$ (N)	Optimal Muscle Fiber Length $L_o^m$ (m)	Tendon Slack Length $L_s^t$ (m)	Pinnation Angle $\alpha$ (deg)
Iliopsoas	1474	0.1269	0.0850	7
Gluteus Medius & Minimus	2686	0.0760	0.0355	10.4
Hamstring	2340	0.4065	0.3850	8.7
Vasti	6482	0.1096	0.2250	4.5
Gastrocnemius	1423	0.0482	0.4250	14.8
Soleus	3599	0.0243	0.2700	25
Dorsiflexors	1400	0.1009	0.2250	6.9

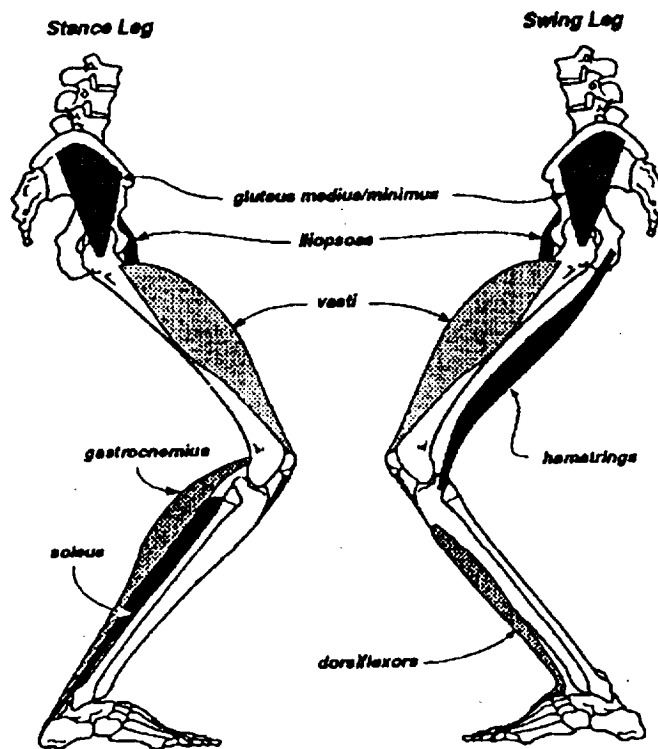


Figure 5.8: Minimal Set of Ten Musculotendon Actuators as Determined by Yamaguchi

functions of the state variables, i.e. the generalized coordinate,  $q_i$ . As stated earlier, the attachment of the musculotendon to bone is specified by the defining an origin, the proximal attachment, and an insertion, the distal attachment. Effective origins and effective insertions are specified when the straight path from the actual origin to actual insertion passes through bone or out of anatomical range during certain body configurations. Origins and insertions are specified with respect to coordinate systems which are directed along the bones and are fixed with respect to the foot, shank, thigh and pelvis. The origin and insertion points for the 7 muscle groups used in this analysis are given in Table 5.5. We used the same origins, insertions and pathways as utilized by Yamaguchi in his model which were defined according Brand *et al.* (1982) and Hoy *et al.* (1990).

Table 5.5: Origins and Insertions of the Musculotendon Groups.  $X$ ,  $Y$  and  $Z$  axes correspond to pelvic, femoral, tibial and foot coordinates system (see Figure 5.9). The foot reference frames is the same as the tibial reference frame at anatomical position. Subscripts  $a$  and  $e$  refer to actual versus effective origins/insertions.

Musculotendon	Point	X (m)	Y (m)	Z (m)	Reference Frame
Iliopsoas	$O_a$	0.0075	0.1350	-0.0400	pelvic
	$O_e$	0.0260	0.0293	-0.0042	pelvic
	$I_a$	-0.0180	0.3351	0.0116	femoral
Gluteus Medius & Minimus	$O$	-0.0155	0.0785	0.0076	pelvic
	$I$	-0.0159	0.3873	0.0589	femoral
Hamstring	$O_a$	-0.0409	-0.0455	-0.0140	pelvic
	$I_a$	-0.0170	0.3800	0.0073	tibial
Vasti	$O_a$	0.0106	0.2026	0.0205	femoral
	$I_a$	0.0170	0.3930	-0.0006	tibial
Gastrocnemius	$O_a$	-0.0203	0.0071	-0.0073	femoral
	$I_a$	-0.0368	-0.0429	0.0028	foot
Soleus	$O_a$	-0.0268	0.2467	0.0006	tibial
	$I_a$	-0.0365	-0.0428	0.0056	foot
Dorsiflexors	$O_a$	-0.0155	0.2175	0.0134	tibial
	$O_e$	0.0259	0.0117	-0.0093	tibial
	$I_a$	0.1035	-0.0520	0.000	foot



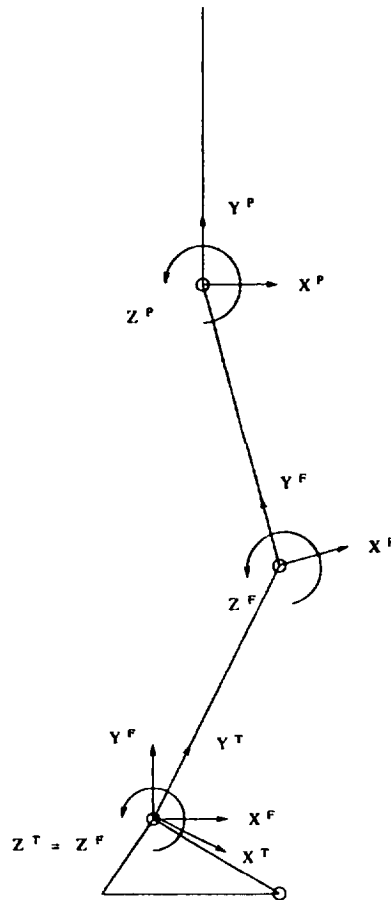


Figure 5.9: Definitions for the Foot, Tibial, Femoral and Pelvic Frames

### 5.5.3 Calculation of Musculotendon Length, Velocity and Moment Arm

The total length and velocity of the musculotendon complex, which is needed as input into the musculotendon dynamics, can be derived for most muscles through vector addition. In this case, the length of the musculotendon is given by

$$L^{mt} = |\overrightarrow{O_a O_e}| + |\overrightarrow{O_e I_e}| + |\overrightarrow{I_e I_a}| \quad (5.5)$$

where  $O$  and  $I$  refer to origin and insertion, and the subscripts  $e$  and  $a$  refer to actual and effective coordinates. The velocity of the musculotendon is then just the time derivative of the length.

Musculotendon forces were incorporated into the body dynamics as joints torques. When a musculotendon spans a joint  $J$ , a joint torque is realized across that joint. The joint torque due to musculotendons which do not span the knee are computed using standard vector cross product methods. In this case, the moment  $\vec{M}$  acting on the proximal segment is defined as follows

$$\vec{M} = \pm F^t \left( \vec{p} \times \frac{\vec{O_e I_e}}{|\vec{O_e I_e}|} \right) \quad (5.6)$$

where  $\vec{p}$  is a vector from the joint to a point on the line of action of the musculotendon, and the line of action is defined by the unit vector

$$\frac{\vec{O_e I_e}}{|\vec{O_e I_e}|},$$

the tension in the musculotendon complex,  $F^t$ , is produced according to equation (4.14), and the symbol  $\times$  represents a vector cross product (see Figure 5.10). The cross product,

$$\vec{m}_e = \vec{p} \times \frac{\vec{O_e I_e}}{|\vec{O_e I_e}|},$$

represents the effective moment arm associated with the musculotendon at a certain body configuration. The sign in equation (5.6) depends on whether the musculotendon acts to extend or flex the joint it spans.

This general method works well for all muscle which do not span the knee. The complication which arises for those musculotendons which do span the knee (Vasti, Hamstring, and Gastrocnemius) occurs because of the complexity of the knee joint. In short, as the knee flexion angle varies this produces both a change in the location of the knee joint center and in the location of the patella. Since this complexity is not accounted for in the simple segmental model formulated here, it is best to use alternative methods to the vector methods discussed above when defining effective moment arms and the lengths of these musculotendons. As an alternative, we defined the effective moment arms of the Vasti, Hamstring and Gastrocnemius according to curves which were formulated by Yamaguchi from a planar model of the knee developed by himself and Zajac (1989). These curves

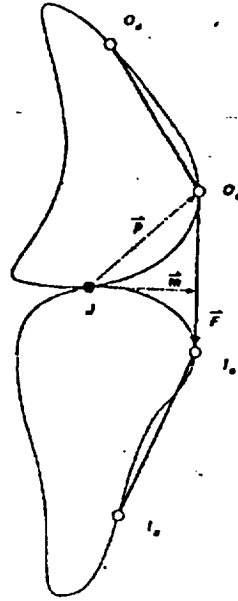


Figure 5.10: Muscle Pathway and Effective Moment Arm [Yamaguchi]

define the moment arms as functions of the knee flexion angle (see Figures 5.11 through 5.13). Thus the joint moments produced by these musculotendons which span the knee are given by

$$\vec{M} = \pm F^t \cdot m_e(\theta_f) \quad (5.7)$$

where  $F^t$  is produced according to equation (4.14) and  $m_e$  is the effective moment arm as a function of the knee flexion angle,  $\theta_f$ .

We then calculated the length of these musculotendons by integration of the moment arm (Wendt and Johnson, 1985; Hoy *et al.*, 1990; Yamaguchi, 1989). In this method, the relationship between the length of the musculotendon ( $L^{mt}$ ), the effective moment arm ( $m_e$ ) and the joint angle is given by

$$v^{mt} = \frac{dL^{mt}}{dt} = m_e(\theta_f) \frac{d\theta_f}{dt}. \quad (5.8)$$

Thus three more differential equations are added to the system.

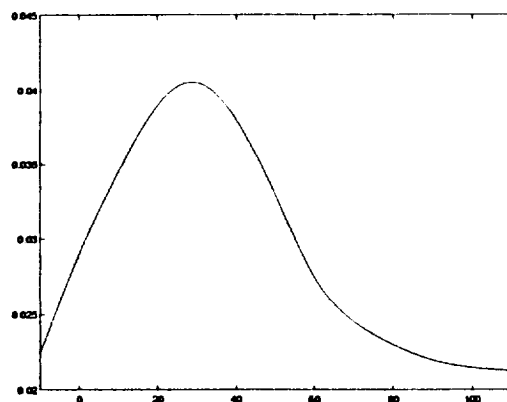


Figure 5.11: Effective Moment Arm of Vasti as a Function of Knee Flexion

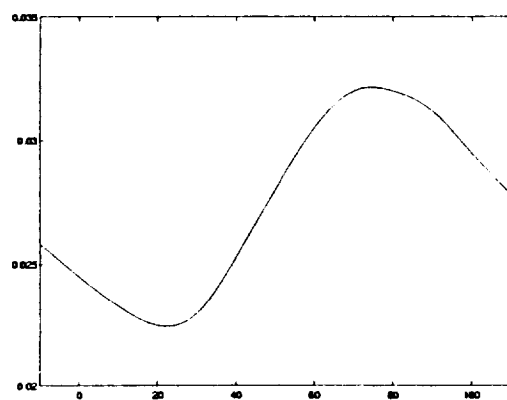


Figure 5.12: Effective Moment Arm of Hamstring as a Function of Knee Flexion

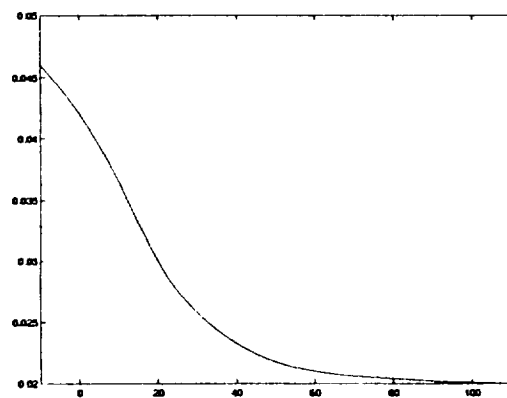


Figure 5.13: Effective Moment Arm of Gastrocnemius as a Function of Knee Flexion

### 5.6 Controls for the Musculotendon Actuators

As stated earlier, when a direct-dynamic analysis of gait driven by musculotendon actuator is to be simulated, musculotendon controls must be derived. Developing these controls constitutes one of the most difficult aspects in forward gait analyses. Thus one of the advantages of mimicking Yamaguchi's model was that his controls, with minor alterations, could initially be used to produce loading conditions needed in our analysis of the long bones.

Some form of dynamic optimization is usually utilized in developing controls for a forward analysis. Yamaguchi produced his controls through a two-phase process: (1) coarse optimization of controls and (2) fine-tuning via trial-and error. The first phase used the dynamic programming of Bellman (Kirk, 1970; Larson and Casti, 1978) to determine the minimal set of muscles needed in the simulations and a crude estimation of muscle *activation*. During this process, Yamaguchi's model was simplified significantly to ease the computational cost associated with dynamic programming; this included discretizing the state space.

Dynamic programming offered Yamaguchi a couple of advantages over other optimization schemes. This approach allows the control to be dynamically optimized over the entire time interval as opposed to being optimized in a quasi-static fashion (Yamaguchi, 1989). Another advantage is that dynamic programming does not require the linearization of the dynamic equations of motion, nor do bounded controls present a problem.

The cost function used in the dynamic programming consists of a error tracking term so that deviation from the nominal trajectory are penalized and a term which seems to be related to muscle fatigue (Crowninshield and Brand, 1981)

$$J_i(k) = \sum_{l=1}^{2n} w_{x,l} (x_l - x_{l,des})^2 + \sum_{l=1}^m w_{u,l} \left( \frac{F_l^t}{PCS A_l} \right)^3. \quad (5.9)$$

In equation (5.9),  $x_l$  is one of the  $2n$  elements comprising the state variable,  $\vec{X} = (q_1, q_2, q_3, q_4, q_5, q_6, q_7, q_8, \dot{q}_1, \dot{q}_2, \dot{q}_3, \dot{q}_4, \dot{q}_5, \dot{q}_6, \dot{q}_7, \dot{q}_8)$  (refer to Figure 5.1) associated with the body,  $F_l^t$  and  $PCS A_l$  are the force and physiological cross-sectional area of muscle  $l$ , and  $m$  is the number of muscles considered originally in

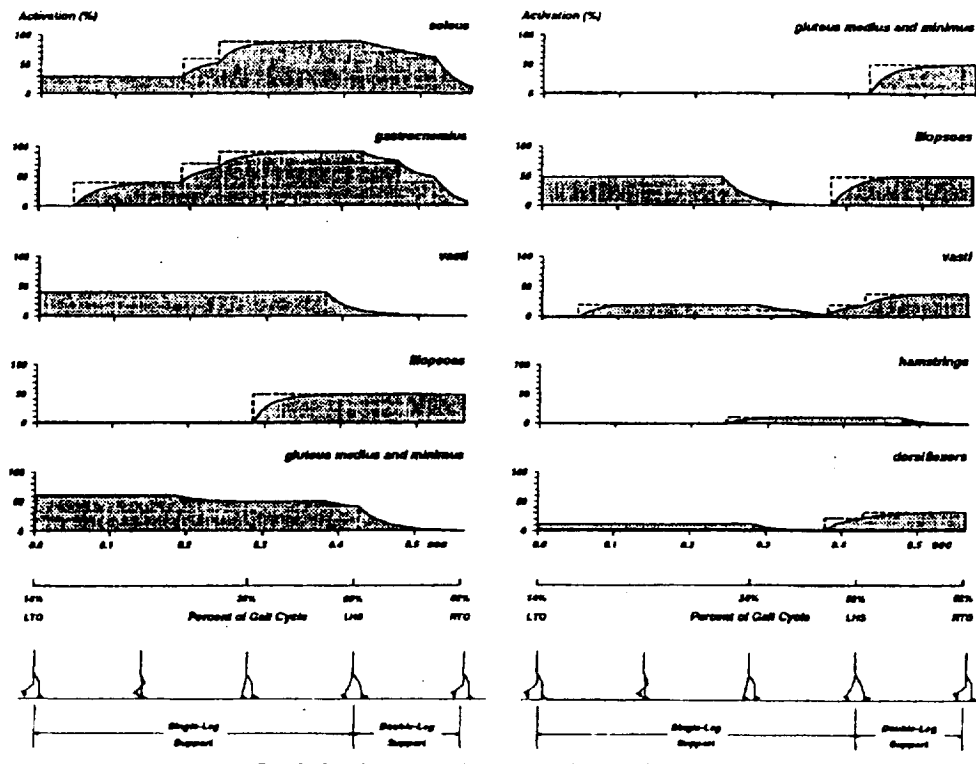


Figure 5.14: Control  $u(t)$  (dashed lines) and activation  $a(t)$  (shaded curves) for the ten musculotendon actuators used in Yamaguchi's dissertation [Yamaguchi]

Yamaguchi's research. The nominal gait trajectories were contained in  $x_{l,des}$  and were specified according to data recorded by Winters (1987) and Inman *et al.* (1981).

Once a minimal set of muscles (see Figure 5.8) and crude *activation* controls were formulated, Yamaguchi ran full model simulations and refined the *neural* controls. The controls Yamaguchi derived are pictured in Figure 5.14. When we ran our simulations, we started with these controls and proceeded to fine-tune them to meet the specific needs of our slightly modified model. As noted by other researchers (Yamaguchi, 1990; Pandy and Berme, 1987), it is surprising that such a complex, coupled and dynamically unstable system can simulate normal gait with such crude and simple controls.

## CHAPTER VI

### DYNAMIC SIMULATIONS

#### 6.1 Numerical Implementation

Until recently a limiting factor on the complexity added to gait models was the difficulty associated with deriving the equations of motion. Kane's vector based method for formulating equations of motion simplified this task, but still derivations done by hand could still take months to perform (Kane and Levinson, 1985). Luckily Kane's method lends itself to computer implementation. Programs now exist which are proficient in algebraic manipulations and Kane's method (SYMB, by Nielan, 1986; AUTOLEV, by Schaechter and Levinson, 1987). These programs are able to calculate the entire set of dynamic equations in algebraic form for open-chain linked-segment models, making it possible to utilize models with more segments and more degrees of freedoms.

AUTOLEV was our choice of program because it provides a step by step approach to Kane's method which allows some insight into the nature of the equations derived. As stated in the user's manual (Kane and Levinson, 1996), "AUTOLEV was created expressly to facilitate analyses based either on Kane's method or on Newton-Euler equations." In addition, AUTOLEV produces efficient programs in FORTRAN or C for the numerical solution of ordinary, nonlinear differential and or non-differential equations. Thus AUTOLEV was considered to be a valuable tool with regards to this research.

A brief description of how AUTOLEV formulates equations of motion may be of value. As stated earlier, AUTOLEV allows the user to perform Kane's step-by-step method online. Kane's method, also known as Lagrange's form of D'Alembert's principle (Ju and Mansour, 1988), is based on dynamical equations of the form

$$\tilde{F}_r + \tilde{F}_r^* = 0 \quad (r = 1, 2, \dots, p) \quad (6.1)$$

where  $\tilde{F}_r$  are the *constrained generalized active forces* and  $\tilde{F}_r^*$  are the *constrained generalized inertial forces* for a system  $S$  possessing  $p$  degrees of freedom in a Newtonian reference frame  $N$ . The constrained generalized active forces are defined

as

$$\tilde{F}_r \equiv \sum_{i=1}^v \tilde{v}_r^{P_i} \cdot R_i \quad (6.2)$$

where  $v$  is the number of particles (or segments) that form  $S$ ,  $P_i$  ( $i = 1, \dots, r$ ) are the particles (or segments),  $\tilde{v}_r^{P_i}$  ( $r = 1, \dots, p$ ) are the constrained partial velocities of  $P_i$  in the reference frame  $N$ , and  $R_i$  is the resultant of all contact forces (such as ground reaction forces) and distal forces (such as gravitational forces). The constrained generalized inertial forces are defined by

$$\tilde{F}_r^* \equiv \sum_{i=1}^v \tilde{v}_r^{P_i} \cdot R_i^* \quad (6.3)$$

where  $R_i^*$  is the inertial force for  $P_i$  in reference frame  $N$ ; that is,

$$R_i^* \equiv -m_i a_i \quad (6.4)$$

where  $m_i$  is the mass of  $P_i$  and  $a_i$  is the acceleration of  $P_i$  in reference frame  $N$ .

Equation (6.1) is equivalent to Newton's second law of motion (Kane and Levinson, 1996). Indeed if  $R_i$  is the resultant of all contact forces and distance forces acting on a typical particle  $p_i$  of the system  $S$ , and  $a_i$  is the acceleration of  $P_i$  in a Newtonian reference frame  $N$ , then in accordance to Newton's law the equations of motion are given by,

$$R_i - m_i a_i = 0 \quad (i = 1, \dots, v) \quad (6.5)$$

where  $m_i$  is the mass of  $P_i$  and  $v$  is the number of particles of  $S$ . Dot-multiplication of equation (6.5) with the partial velocities  $\tilde{v}_r^{P_i}$  of  $P_i$  in  $N$  and subsequent summation yields

$$\sum_{i=1}^v \tilde{v}_r^{P_i} \dot{R}_i + \sum_{i=1}^v \tilde{v}_r^{P_i} \cdot (-m_i a_i) = 0, \quad (r = 1, \dots, p), \quad (6.6)$$

which is indeed equivalent to equation (6.1) by the definition stated in equations (6.2), (6.3) and (6.4).



When using AUTOLEV, one follows a simple recipe to obtain the equations of motion:

- Declare a *Newtonian* Reference frame *N*.
- Declare *bodies, frames, points, and particles*, specifying their mass and inertial characteristics.
- Declare *generalized speeds* and their time-derivatives.
- Declare *generalized coordinates* and their time-derivatives.
- Create the *kinematic differential equations* by relating the time-derivatives of the generalized coordinate to the generalized speeds.
- Form *position vectors* and *directional cosine matrices*.
- Form *angular and linear velocities*, which AUTOLEV can do for you.
- Impose *motion constraints*, if necessary.
- Form *angular and linear accelerations*, which AUTOLEV can also do for you.
- Enter expression for *forces and torques*.

Once these components are entered, AUTOLEV can generate the equations of motion and FORTRAN or C code which will integrate these equation forward in time using a fourth-order Runge Kutta integration scheme. In our model, the influences of the muscles were realized as torques entered about the joints, and ground reaction forces were entered as forces applied to the heels. Most of the components of the musculotendon dynamics were entered into AUTOLEV directly; however, some issues, such as the controls and the spline approximations to various curves, were entered directly into the C code in the form of subroutines.

One of the additional benefits in using AUTOLEV was its ability to find instantaneous loading conditions needed in our finite element code to analyze the stresses in long bone. Once the equation of motion were generated, one could specify additional generalized speed, properly constrain them and then solve for the contact

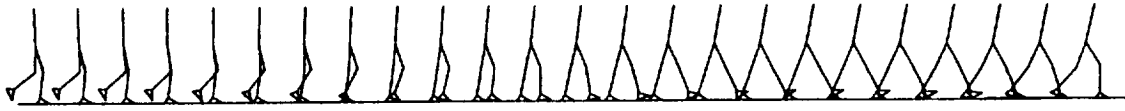


Figure 6.1: 2-Dimensional Representation of Our Gait Simulation

or joint reaction forces found at the distal and proximal ends of the segments. AUTOLEV was also able to resolve the tangential components of the muscle forces along the bones, which enabled us to specify surface tractions along the bone.

## 6.2 Dynamic Simulation

Most simulations were performed on the Digital Alpha workstation. The average time needed to perform a full simulation was approximately 3 hours. Many simulations were ran before the model performed appropriately. Figure 6.1 shows the graphics corresponding to one of the better simulations. Notice that the figures do appear to mimic normal gait, with a few exceptions which will be discussed later.

For obvious reasons, the simulation and many of the results reported in this section are very similar to the results reported by Yamaguchi. However, since our models do differ slightly, e.g., we used different muscle models, slight variations do occur and shall be pointed out to the reader.

### 6.2.1 Controls and Initial Conditions

As stated earlier, one of the reasons for utilizing Yamaguchi's model was that the basic controls laws needed for a gait simulation were already formulated. We thought that this would accelerate the rate at which we could arrive at the loading conditions needed for our continuum analysis of the bones. In retrospect, it is not clear that this did indeed speed up the process. This is because it is hard to mimic such a complex process when all details are not clearly defined. The degree to which small variations in the model affect the overall performance of the

simulation is hard to define, and one is left wondering if variations are due to the slight differences or if a fundamental element has been neglected or misinterpreted.

With that said, we found that our final model did indeed mimic the overall performance of Yamaguchi's model quite adequately, and our control laws varied only slightly from the original set as published by Yamaguchi (1989). The final version of our controls for each musculotendon unit are illustrated in Figure 6.2. The reader is referred back to Figure 5.14 to evaluate the differences between these two control sets.

One possible explanation for some of the differences could be the variation of the muscle model used. In Yamaguchi's dissertation, there is a schematic diagram depicting the Hill type musculotendon model he utilized. In this diagram, a series elastic element within the muscle is depicted; however, no further information on the approximate form of this elements was given. As a result, we choose to ignore this feature. Thus our musculotendon actuator undoubtedly reacts somewhat differently from his. It should be noted that Zajac gives some fundamental reasons which validate the exclusion of this element, in that it's inclusion raises issues about the constituency of the basic notion that sarcomeres and fibers act in concert. Zajac also states that in most instances tendon compliance dominates and that the elastic element in muscle can be neglected (Zajac, 1989). Thus we felt justified in the exclusion of this element from our musculotendon model.

Another possible explanation for the differences needed in our simulation could be the result of the variance in the initial conditions used to start the simulation. In order to start the simulations, the program must be provided with the initial segmental orientations ( $q_1, \dots, q_8$ ), the initial angular speeds ( $\dot{q}_1, \dots, \dot{q}_8$ ), the initial force in each musculotendon, and the initial lengths of the musculotendons which spanned the knee joints whose lengths were found using the moment arm integration method. Since initial conditions were not specified in Yamaguchi's dissertation, we took educated guesses at what the model's initial segmental orientation should be by studying Yamaguchi's figures and graphs and then by referring to the gait data reported by Winter (1987). The initial force in each musculotendon was found by running mock simulations to find the steady state muscle force achieved by the initial control when the motion of the model was constrained. Finally the

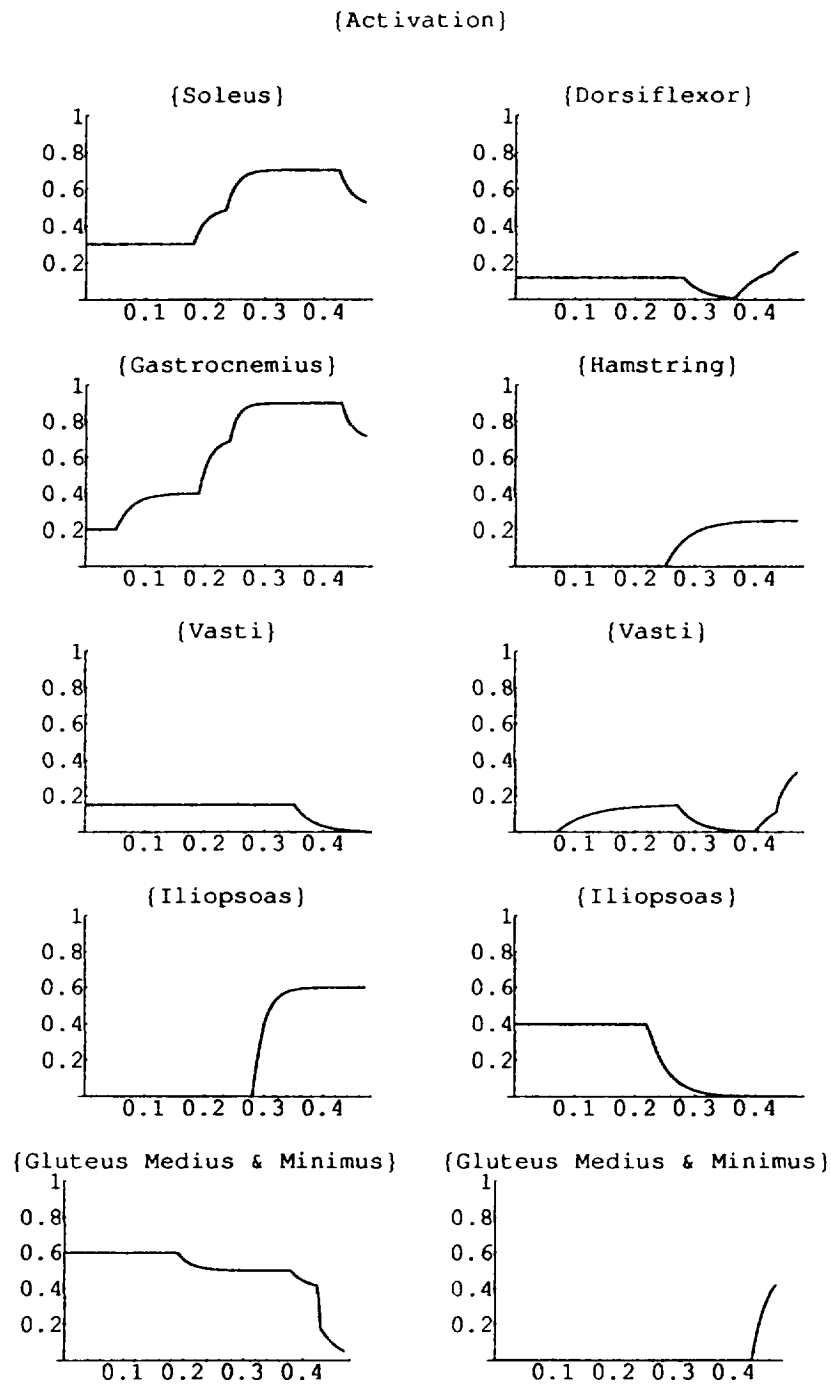


Figure 6.2: Controls Utilized in Simulation

initial lengths for the musculotendons which crossed the knee were determined by trial and error. We sought an initial length of the musculotendon such that the muscle maintained an appropriate length throughout the gait cycle. The initial conditions defined for the angular velocity of the segments was crucial for a proper simulation of gait. Of particular importance was the initial sagittal plane velocity of the HAT. Due to its enormous mass, errors here were hard to overcome. Table 6.1 defines our initial conditions.

### 6.2.2 Joint Angles and Joint Torques

A standard means of comparing and validating gait simulations is achieved by displaying the joint torques which drive the system and the resulting joint trajectories. Figure 6.3 depicts the standard definitions of the joint angles. Notice that these joint angles are distinct from the generalized coordinates used in the analysis. Figure 6.4 displays the resulting joint trajectories in our simulation. Although these trajectories appear to be in good qualitative agreement with the trajectories reported by other researchers (Yamaguchi, 1989; Winter, 1987; Inman *et al.*, 1981), there are some critical areas of concern. One such area is the slight hyperextension of the stance leg knee joint. Another area of concern is the exaggerated flexion of the hip.

Joint torques represent the combined effects of the active and passive structures which drive the body. In an effort to describe all the components which accumulate in the total joint torque, two graphs are displayed for each joint angle (see Figures 6.5 through 6.9). The first graph displays the total joint torque and distributions of the active and passive components. The second graph breaks down the active component, i.e., the muscular component, into the individual contributions from each musculotendon unit spanning that joint. The second graph thus gives one an idea of the role played by each musculotendon throughout the gait cycle. It is important to understand that these pictures do not give the whole story in that a torque produced by a muscle spanning one joint can and usually does accelerate all body segments to a lesser or greater extent. This idea of describing muscular function by determining the segmental accelerations caused by each musculotendon was suggested by Zajac and Gordon (1989). We find that our total torques are in

Table 6.1: Initial Conditions for the Gait Simulation

Generalized Coordinates (Degrees)		Generalized Speeds (Radians/Seconds)	
$q_1$	146	$\dot{q}_1$	-0.03
$q_2$	85	$\dot{q}_2$	-1.06
$q_3$	107	$\dot{q}_3$	-2.05
$q_4$	0.0	$\dot{q}_4$	0.00
$q_5$	92	$\dot{q}_5$	-0.41
$q_6$	91	$\dot{q}_6$	-2.85
$q_7$	140	$\dot{q}_7$	-.35
$q_8$	190	$\dot{q}_8$	-1.97
Musculotendon Forces (Newtons)			
Stance Leg		Swing Leg	
$F_{sol}^t$	900	$F_{dor}^t$	130
$F_{gas}^t$	85	$F_{ham}^t$	.5
$F_{vas}^t$	850	$F_{vas}^t$	3
$F_{gmm}^t$	1450	$F_{gmm}^t$	15
$F_{ils}^t$	32	$F_{ils}^t$	630
Musculotendon Length			
$L_{vas_s}^{mt}$		0.3192	
$L_{ham_w}^{mt}$		0.4775	
$L_{vas_w}^{mt}$		0.3199	



Figure 6.3: Joint Angle Definitions

good agreement with Yamaguchi's reported joint torques, and these torques are in general accordance with the data reported by other researchers (Davy and Audy, 1987; Hardt, 1978).

### 6.2.3 Musculotendon Analysis

In this section, the dynamics of each musculotendon unit will be reviewed in terms of the normalized force and power produced by each musculotendon. Figure 6.12 reports the normalized force realized in the tendons of all ten musculotendon actuators. These normalized forces,  $F^t/F_0$ , were obtained through the dynamics described in Chapter V. Although Yamaguchi did not report such results, similar forces are predicted by other authors (Pierrynowski and Morrison, 1985; Brand *et al.*, 1986).

Another means of describing the functions of the muscle, tendon and the complete musculotendon unit is through the analysis of the power trajectories. These trajectories are depicted in Figure 6.13. This power reflects the rate at which the muscles and tendons are expending and absorbing energy. When a muscle or ten-

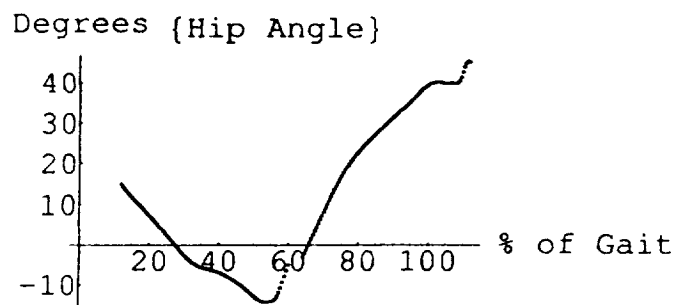
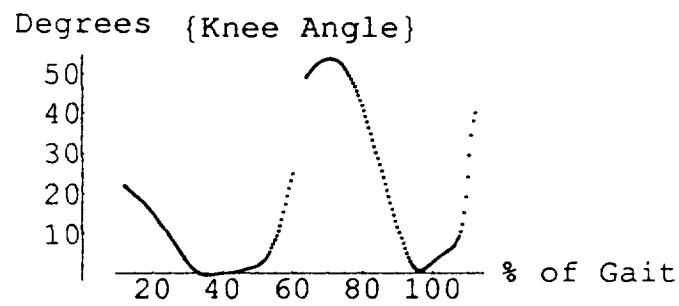
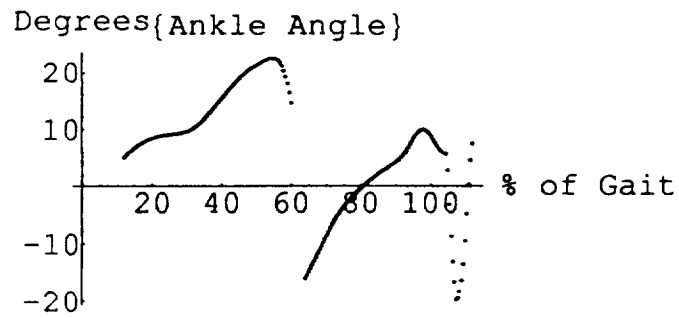


Figure 6.4: Joint Trajectories



{Ankle Plantarflexion}

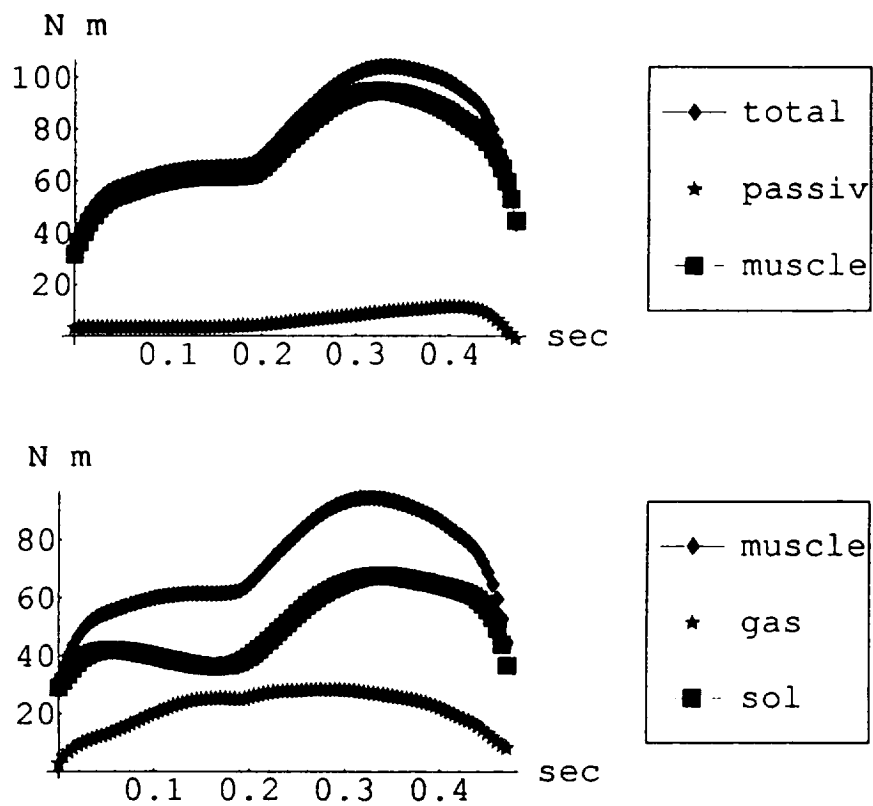


Figure 6.5: Stance Ankle Joint Torque

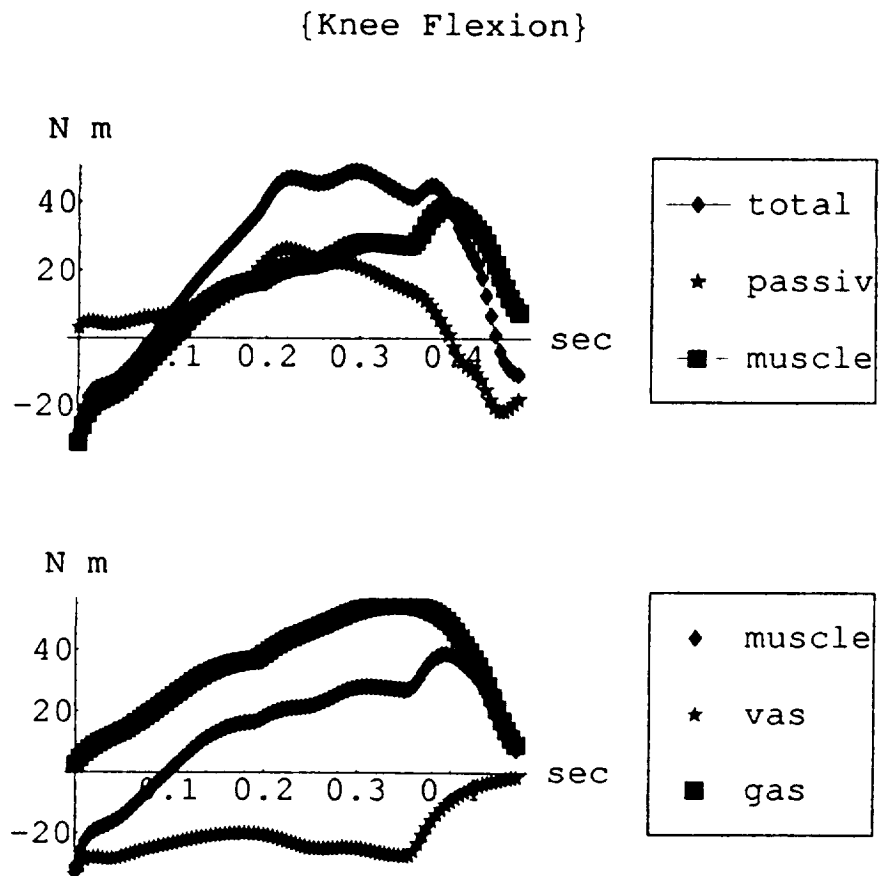


Figure 6.6: Stance Knee Joint Torque

{Hip Extension}

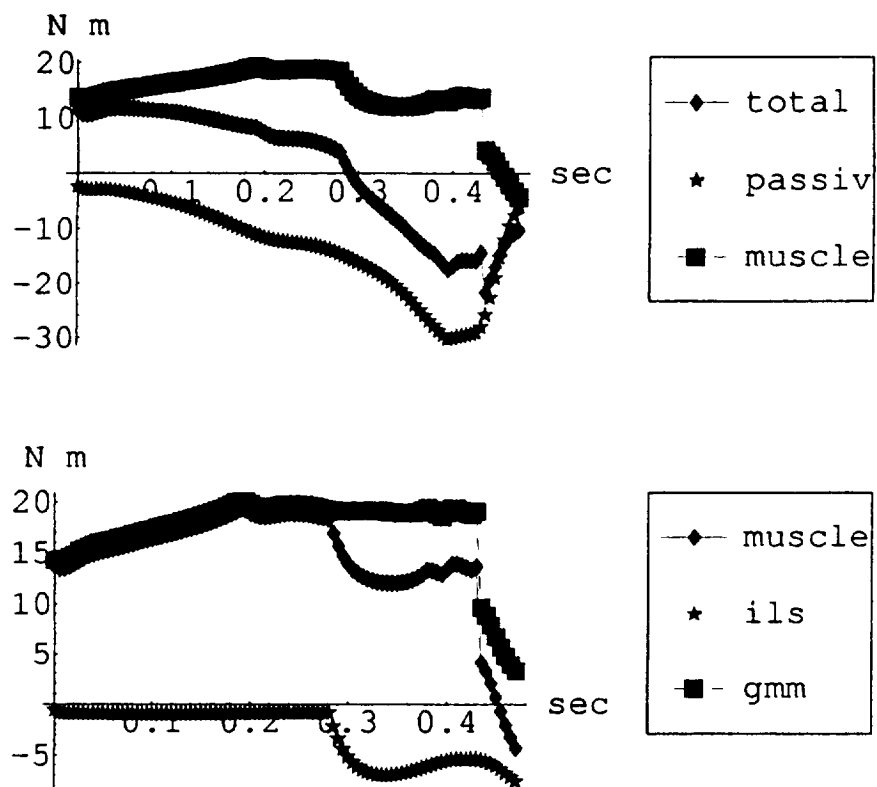


Figure 6.7: Stance Hip Joint Torque for Flexion

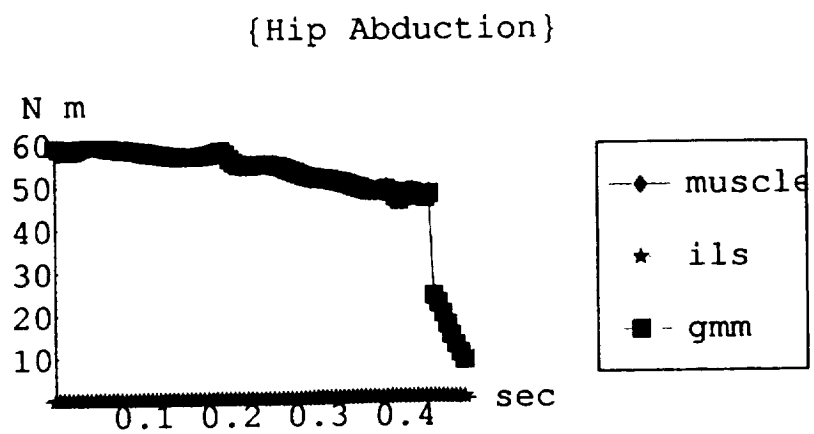


Figure 6.8: Stance Hip Joint Torque for Abduction

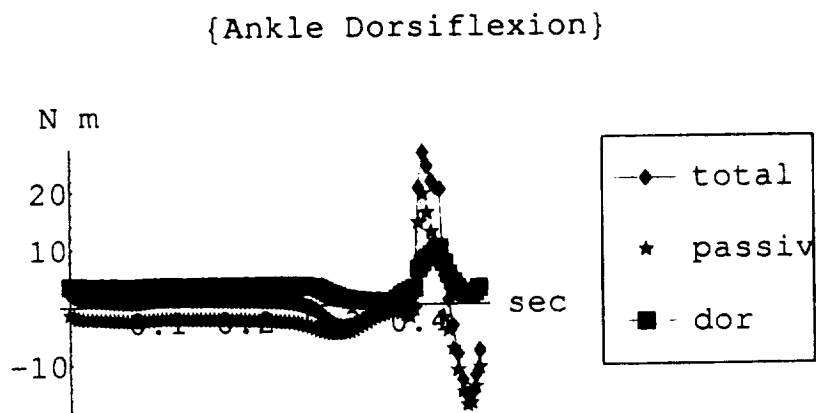


Figure 6.9: Swing Ankle Joint Torque

{Knee Extension}

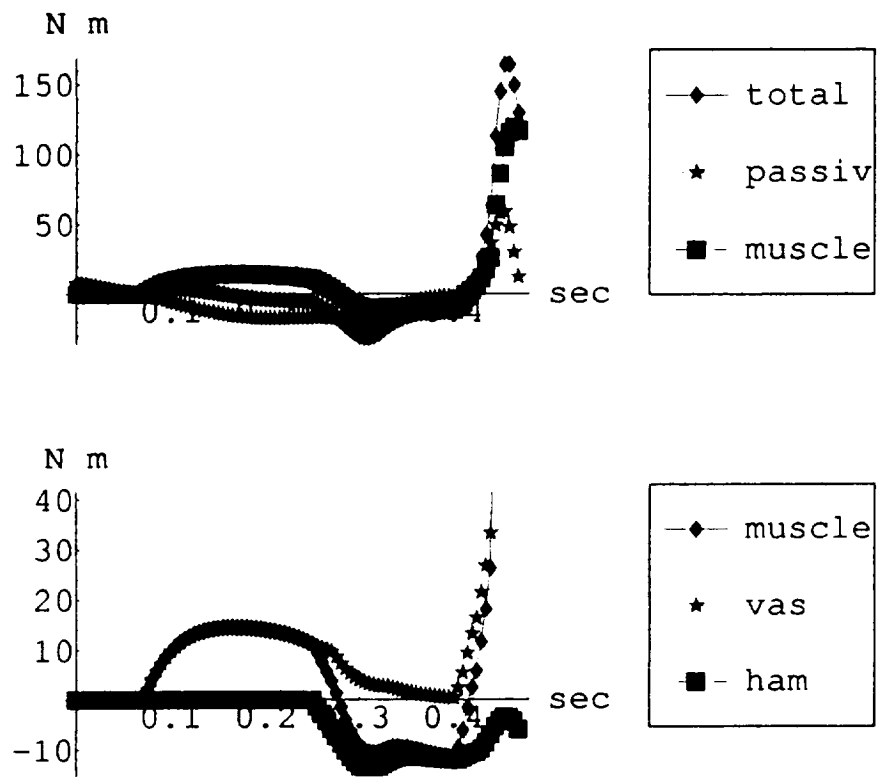


Figure 6.10: Swing Knee Joint Torque

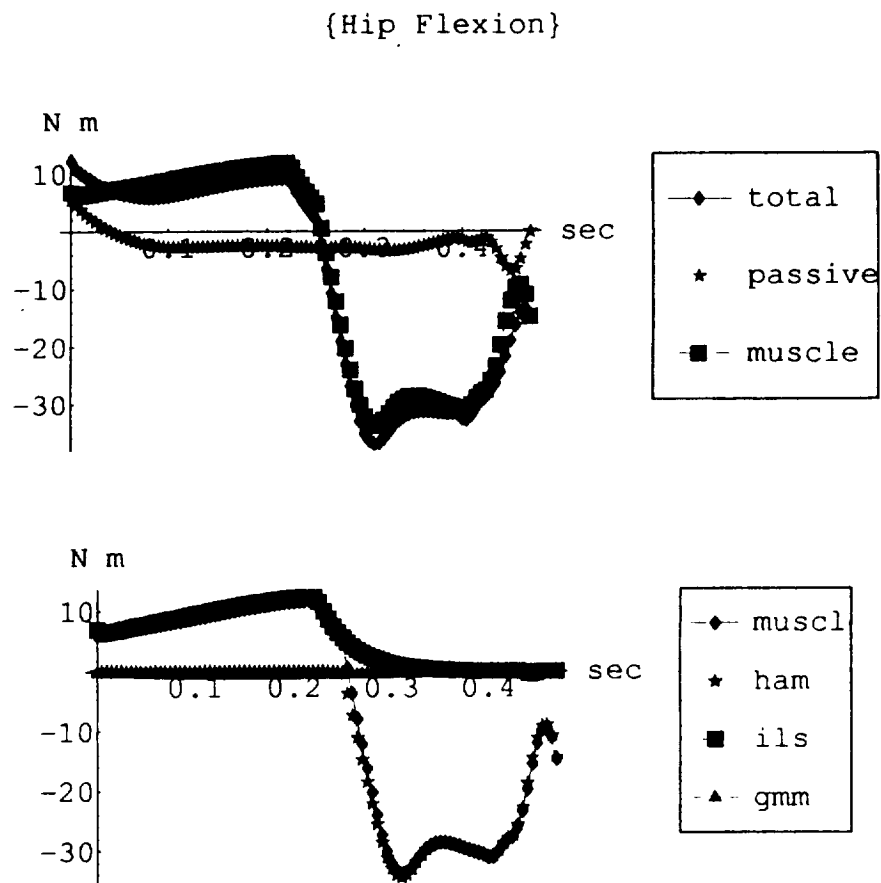


Figure 6.11: Swing Hip Joint Torque

don produces force while shortening, a concentric contraction, energy is released to the system. In contrast, if force is produced while the unit is lengthening, an eccentric contraction, then energy is absorbed or stored. This gives insight into the function of the musculotendons.

To exemplify these ideas, we will examine the power histories of the plantarflexors, the Soleus and Gastrocnemius, of the stance leg. After heel strike of the stance leg and during single leg support the total power, the summation of the powers in the tendon and muscle, of the plantarflexors are predominately negative as they store energy or absorb the weight and maintain the upright position of the leg. However, during the push off phase this power becomes positive as they release this energy to facilitate lift off of the stance leg and the shift of weight to the swing leg during double support. In addition, the hamstring is seen to absorb energy as it brakes the extension of the swing leg.

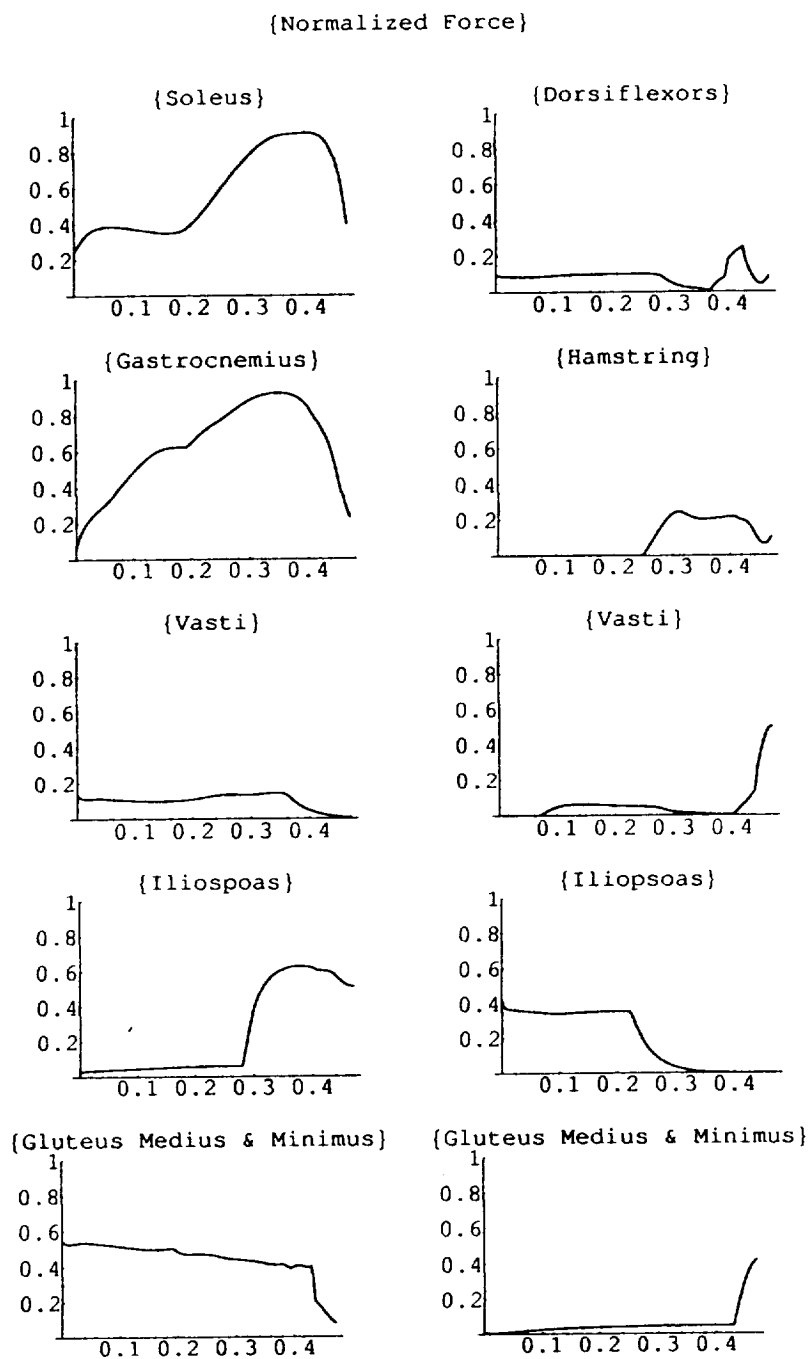


Figure 6.12: Normalized Force Histories for each Musculotendon. Left column refers to stance muscle while the right column refers to the swing side muscles.



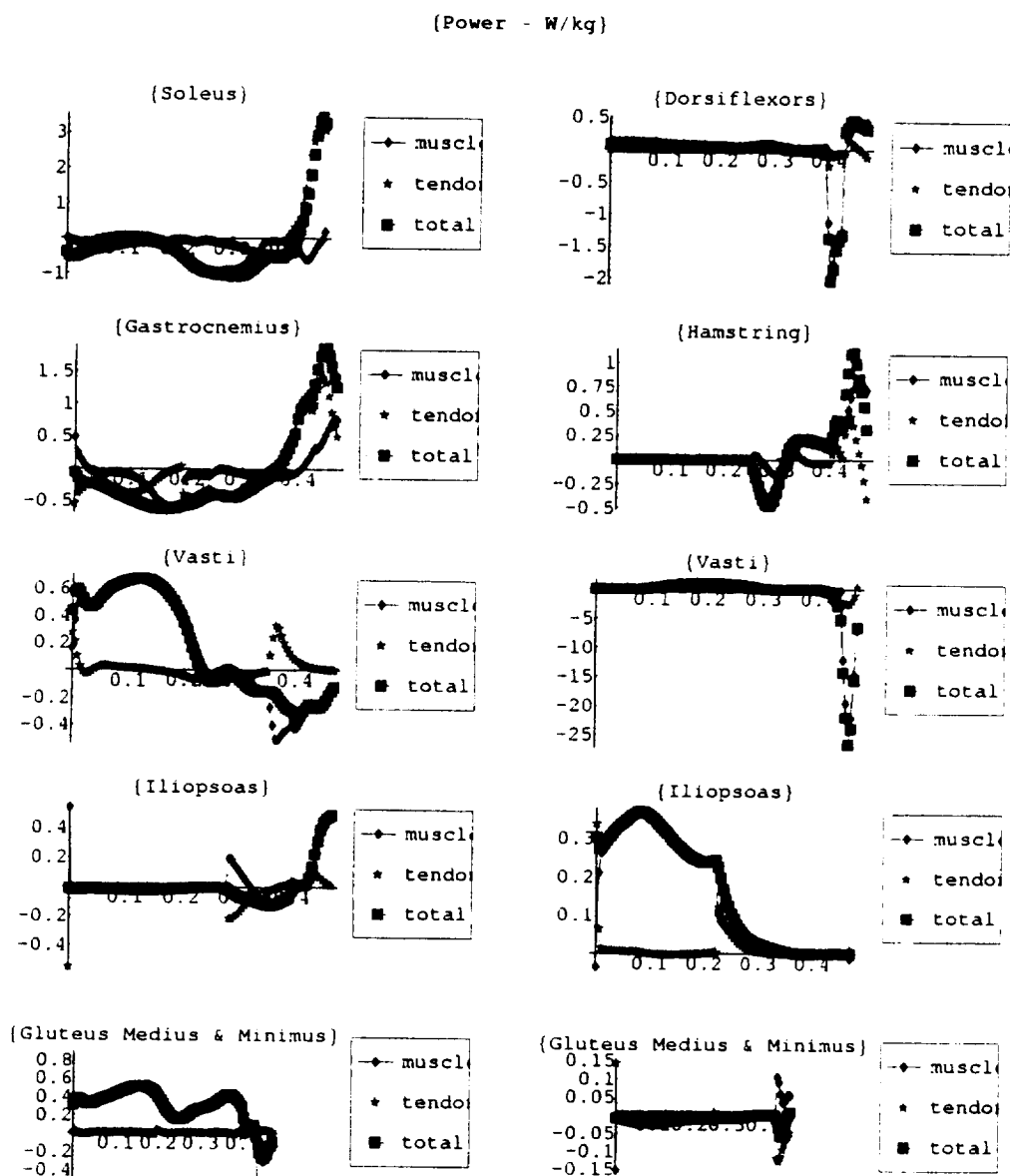


Figure 6.13: Normalized Power Curves for each Musculotendon. Left column refers to stance muscles while the right column refers to the swing side muscles. Positive power corresponds to the rate of energy the muscle expend while performing a concentric contraction. Negative power is the rate of energy the muscle absorbs during an eccentric contraction. All curve are normalized by the weight of the model, 76 kg.

## CHAPTER VII

### A CONTINUUM ANALYSIS OF SKELETAL ELEMENTS

#### 7.1 Introduction to Bone Mechanics

Before giving the results of our continuum analysis of the long bones, it might be beneficial to give a brief summary of some of the issues involved in bone mechanics. First some of the difficulties associated with modeling the skeletal structures will be defined. A brief synopsis of the work which has been done in this field will then be presented. This summary will include the common simplifying assumptions under which bone is modeled. In conclusion, special attention will be given to the research which has attempted to include some of the effects of the musculature in the analysis.

Bone is known to have a complex geometry and nonhomogeneous constitution and these factors are responsible for many of the difficulties associated with defining the mechanical properties of the skeletal members. One only needs to analyze the structure of the femoral head or pelvic girdle to appreciate the nonstandard geometry inherent in bone. With regards to the nonhomogeneity of bones, it is known that bone is the composition of three different materials. The hard outer shell is referred to as cortical or compact bone while the interior of the bone is composed of cancellous bone, also referred to as trabecular or spongy bone, and bone marrow. Trabecular bone is a very complex material which is noncontinuous even on a macroscopic level and is best described as a structure not a material (Huskey and Chao, 1983). Thus bone is most accurately described as an anisotropic, nonhomogeneous material.

Before giving a brief review of some of the current work, it should be noted that bone mechanics is not a new area of research. Some of the classical studies which are cited often are the products of Wolff (1870, 1892) and Koch (1917). Wolff postulated that the patterns seen in the trabecular of bone are aligned with the principal stress fields developed in the bone. This hypothesis became known as "Wolff's Law" and research continues to be conducted in an effort to substantiate this idea (Hayes *et al.*, 1982; Koch, 1917; Rybicki *et al.*, 1972). Later, Koch did some ground breaking work as he gave the first detailed geometric description of

the femur and went on to calculate the stresses induced by loadings which were assumed to occur during normal activities. This work was a landmark in that it was the first attempt to model the bone as a beam and the first to attempt to include some effects of the musculature on the stresses and strains. Although Koch underestimated the joint and muscle forces (Duda *et al.*, 1997), he still concluded that that muscular action could reduce the bending stresses (Koch, 1917; Rybicki *et al.*, 1972).

Since then many studies have followed Koch's lead by modeling the bone as a beam. Viano *et al.* (1976) assumed that the femur was isotropic and modeled it as a hollow cylinder. While Piziali (1976) modeled the tibia as a cantilever beam fixed at the knee and loaded at the ankle. He suggested that bone be viewed as transversely isotropic, that is bone displays one set of elastic properties in one direction and a second set in the perpendicular plane. Thomsen (1990) modeled the tibia as straight, twisted non-uniform Timshenko beam. He viewed the compact bone and cancellous bone as homogeneous, linearly elastic, transversely isotropic material, while bone marrow was consider completely flexible. Thomsen concluded that the stiffness of the trabecular can be ignored, the twist of the tibia is insignificant and thus that a simplified approach modeling the tibia as a uniform beam using mean cross-sectional properties can be justified as long as shear deformations are considered. There are many more authors who have modeled the long bones as beams (Cowin *et al.*, 1985; Huskies, 1983; Salathe *et al.*, 1989). This should give one a feel for the general assumptions made while studying the mechanical characteristics of bone.

Finite element techniques were introduced into the field of bone mechanics in 1972 about fifteen years after their conception into engineering mechanics (Huskies and Chao, 1983). The usefulness of this technique resides in its ability to handle complex geometries and nonhomogenous materials. For a nice review on the progress of FE techniques in orthopedic biomechanics throughout the first decade of its use, the reader is referred to the paper written by Huskies and Chao (1983). Rybicki *et al.* (1972) did a comparison of beam theory and a continuum theory in the form of a finite element program when he studied the femur. This analysis is of particular interest to this dissertation because Rybicki did study the effects

of certain muscle groups on the distribution of stress and internal moments. He concluded that while classical beam theory is appropriate in the shaft of the femur it is inaccurate for regions of the greater trochanter, femoral head and areas of muscular attachment. He also stated that muscles have a pronounce effect on the maximum stress and total strain energy of the femur. Thus we are encourage to pursue a continuum analysis.

As stated above, there is particular interest in the research that has attempted to included the effects of the muscular system into the loading criteria. This dissertation is interested in the response of bone to natural settings where muscular activity plays a role. Unfortunately, it is often hard to define these natural loading conditions. The determination of muscular forces is nontrivial, as was discussed in Chapter II. As a result, most studies have focused on the *in vitro* response of bone to artificially applied loads (Collier *et al.*, 1982; Curry, 1959; Viano *et al.*, 1976; Reilly and Burstein, 1975); however, there are some studies which have attempted the inclusion of normal loading conditions (Duda, 1997; Koch, 1917; Lanyon and Smith, 1970; Orne and Manke, 1975; Toridis, 1969; Sharkey, 1995, Rybicki, 1972). The studies of Koch and Rybicki have already been mentioned, but it should be noted that the muscular forces they utilized were not derived from a particular task. Toridis (1969) developed a theory in which the bone is modeled as a three dimensional elastic beam where muscular force can be included along the bone as point attachments. Although the theory of how to compute these stress field is presented, a detailed example of its application is absence and the reader is not informed on the effects of the muscular forces into the analysis. Sharkey (1995) conducted an *in situ* experiment studying the metatarsal strain in cadaveric feet in an attempt to characterize the development of metatarsal stress fractures which occur frequently in the army. By simulating physiological loading and contraction of the plantar flexors, he was able to conclude that the fatigue of the flexors have a profound effect of the development of stress fractures. Lanyon and Smith (1970) conducted *in vivo* experiments by placing strain gauges on the tibial shafts of sheep. Among their conclusions is the statement that local deformation that culminate in fracture are in many case the result of uncoordinated muscular action. Fortunately or unfortunately, these types of studies are unethical in human analysis, and one

must resort to other means to derive the loading conditions for normal activity. Duda (1997) in his paper entitled, "Internal Forces and Moments in the Femur During Walking," attempted to do just this. In this paper, he included the effects of "all thigh muscles, body weight and contact forces." The muscle forces were taken from the work of Brand (1982, 1986). Thus were derived using a "static" optimization technique as described in Chapter II. Although Duda states that this was not a continuum analysis, it is unclear from the paper how he modeled the femur. Regardless, he does conclude that the muscles play a substantial role in balancing the loads within the femur.

## 7.2 Finite Element Analysis of Tibia

It is a contention of this research that the interrelationship between neural control, applied muscle forces and the resulting motion of body segments influences the development of stress in skeletal members. To explore this notion, a continuum analysis of the tibia will be carried out in which the boundary inputs are derived from the results of the dynamic model of gait. The main point of the approach that is advanced here is that direct dynamics provides instantaneous information regarding the direction and magnitude of muscular forces, net moments at joints and joint reaction forces. This information will be utilized in a stress analysis of the segments that represent the various bones.

To illustrate the mathematical issues involved, a general formulation of the relevant boundary value problem is first presented. In particular, let  $\Omega$  denote a body in  $\mathbf{R}^3$  with boundary  $\Gamma = \Gamma_t \cup \Gamma_d$ ,  $\Gamma_t \cap \Gamma_d = \emptyset$ . For  $u$ ,  $x \in \mathbf{R}^3$ , let  $u(x, t)$  denote the displacement of points  $x \in \Omega$  at time  $t$ . The internal forces, more precisely the stress in  $\Omega$ , may be described in terms of a tensor  $\sigma$  that satisfies the equation of motion

$$\text{div}(\sigma) + f(x, t) = \rho u_{tt}(x, t) \quad x \in \Omega. \quad (7.1)$$

Here  $f(x, t)$  denotes externally applied forces. In the context of the biomechanical situation consider here,  $\Omega$  represents bone and  $f$  corresponds to weight or external surface tractions which are derived from muscular forces. The displacement field must satisfy the equation of motion subject to boundary conditions that are

typically of the form,

$$\begin{aligned}\sigma n &= t, & x \in \Gamma_t \\ u &= \mu_o, & x \in \Gamma_d\end{aligned}$$

where  $n$  denotes an exterior unit vector to  $\Gamma_t$ . Additionally, one must specify a constitutive relation that relates the states of stress to the deformation in  $\Omega$ . Though bone is most accurately modeled as anisotropic material, preliminary work has been carried out under the assumption that bone is isotropic. In this case the components of stress,  $\sigma_{ij}$ ,  $i, j = 1, 2, 3$  may be expressed in terms of displacements by 'Hooke's Law' which states,

$$\sigma_{ij} = 2\mu\epsilon_{ij} + \frac{2\mu\nu}{1-2\nu}\delta_{ij}(\epsilon_{11} + \epsilon_{22} + \epsilon_{33}). \quad (7.2)$$

In the above equation,  $\mu$  and  $\nu$  are elastic parameters and the 'strain' is defined by

$$\epsilon_{ij} = \frac{1}{2} \left( \frac{\partial u_i}{\partial x_j} + \frac{\partial u_j}{\partial x_i} \right). \quad (7.3)$$

Specific problems that correspond to simplified modes of deformation will now be presented.

In the event that a bone experiences a pure tensile or compressive deformation and inertial effects are negligible, it suffices to solve the equation of equilibrium,

$$\frac{\partial}{\partial x} \left( E(x)A(x) \frac{\partial u}{\partial x} \right) + f(x) = 0, \quad 0 < x < l \quad (7.4)$$

where  $E(x)$  denotes Young's modulus,  $A(x)$  the cross sectional area of the bone which has length  $l$ ,  $f(x)$  is an applied surface traction,  $\epsilon(x) = \frac{\partial u}{\partial x}$  is the strain and  $\sigma(x) = E(x)\epsilon(x)$  is the stress. This equation must be solved subject to boundary conditions that reflect the joint reaction forces and specified displacements at the joints.

In this study, the swing leg tibia is analysis at heel strike and flat foot. At these two instances of gait, it is believed that the tibia can be described as undergoing

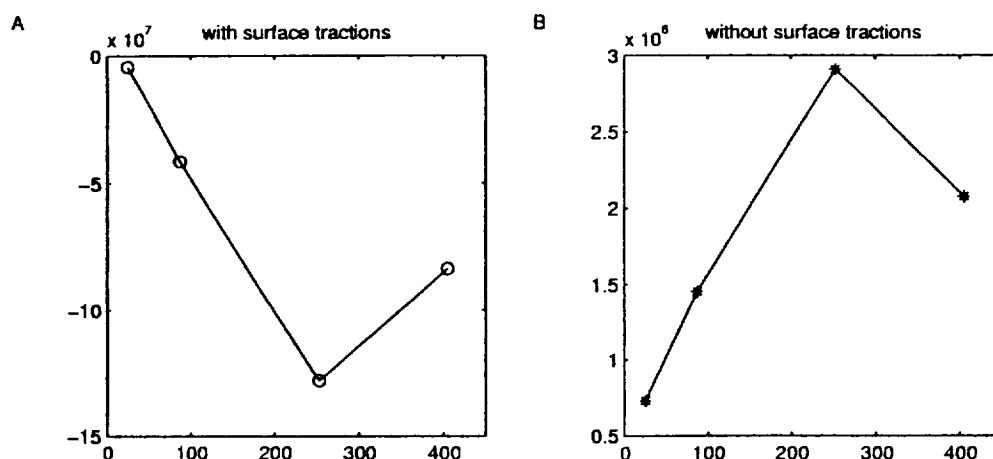


Figure 7.1: Axial Stress Induced During Flat Foot (A) Note that the tibia is in compression when muscular attachments are included in the analysis. (B) When muscular attachments are neglected, the bone is in tension. Note that difference in scales between (A) and (B).

a pure tensile or compressive deformation. The results in Figures 7.1 and 7.2 are finite element approximations to a boundary value problem that correspond to solving equation (7.4) in which  $f(x)$  represents the surface tractions due to muscular loading, in particular the tangential component of the vasti, hamstring and dorsiflexor muscle forces. It was assumed that the distal end of the tibia was fixed at heel strike and flat foot and the boundary condition at the knee joint was given by the normal component of the joint reaction force,  $f_o$ . In particular, the boundary conditions are

$$u(l) = 0 \quad E(0)A(0)\frac{\partial u}{\partial x}(0) = f_o. \quad (7.5)$$

A point to be emphasized is that the inclusion of muscular effects in boundary inputs significantly alter the distribution of stress throughout the bone. This conclusion is supported by other researchers (Duda, 1997; Lanyon and Smith, 1975; Rybicki, 1972; Sharkley, 1995). With the inclusion of muscular attachments portions of the bone are in compression. This is in good qualitative and quantitative agreement with the results of Lanyon (1974) and Duda (1997). This should be

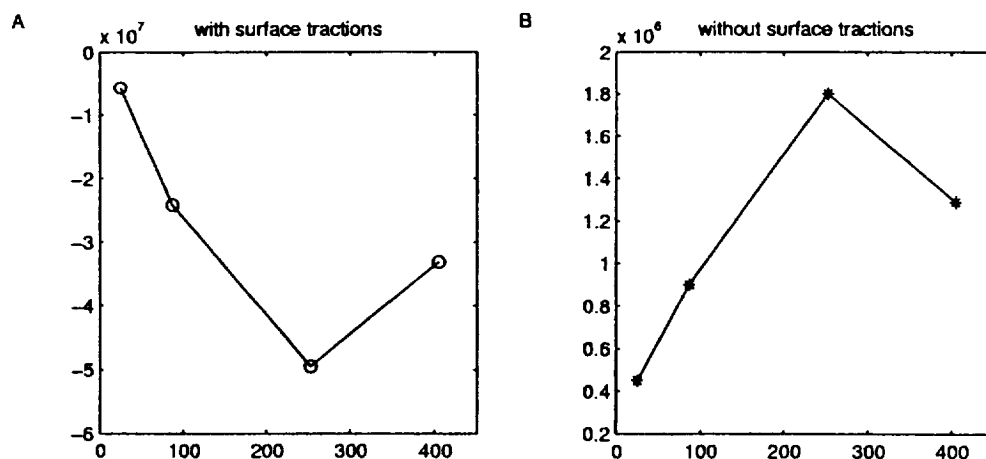


Figure 7.2: Axial Stress Induced During Heel Strike (A) Note that the tibia is in compression when muscular attachments are included in the analysis. (B) When muscular attachments are neglected, the bone is in tension. Note that difference in scales between (A) and (B).

contrasted with the tensile stresses that are predicted when muscular tractions are neglected (see Figure 7.2). The results are not surprising in view of the fact that muscular forces often exceed body weight and thus dominate the loading on bones both at the joints and at the muscle attachment area (Hardt, 1978).

Undoubtedly, more complex modes of deformation must be addressed in order to accurately represent the stress in the bone. Ultimately we intend to utilize 3-D finite element solvers to conduct the stress analysis of the skeletal components. However, a more immediate approach that incorporates the effects of axial, bending and torsional loading will be based on a model of the skeletal system as a configuration of beams in a 3-D structure referred to as a frame. The work done by Toridis (1969) and Rybicki (1972) could serve as templates for this analysis. In this approach, the required boundary inputs would include the distribution of muscular forces along the bone, the normal and tangential components of the joint reaction forces, and the moments at the joints. This data is accessible as output of the dynamic gait model.



## CHAPTER VIII

### CONCLUSIONS

The goal of this dissertation was to define a new method by which the effects of musculature on stress development in the long bones can be ascertained throughout a normal human activity such as walking. As explained in Chapter II, it was a contention of this research that a forward analysis would provide a means by which the instantaneous loading conditions, such as joint reaction forces, joint moments, and muscular forces, of bone could be derived throughout the gait cycle. Since the musculotendon units are central to this approach, it was imperative that a good muscle model be utilized, one that reflected the basic characteristics of muscle while maintaining enough simplicity to render it useful in a simulation. Chapter III explained the key elements that a muscle model should incorporate while Chapter IV presented the model we felt was appropriate for motion simulations. Once the muscle model was determined, we sought a representation of the human body which included enough complexity to mimic the central issues of human gait. It was thought that the model developed by Yamaguchi succeeded in this regard. Chapter V illustrated the construction the complete model and the incorporation of the muscles as actuators in the system. Then Chapter VI reflected on the performance of the model in simulating gait. We felt that the simulations were indeed representative of human gait and that the derived loading conditions were in a reasonable range. Thus we proceeded in Chapter VII to do a finite element analysis of the tibia based on these results. Although modeling the bone as a uniaxial rod is quite simplified and only applicable during certain phases of gait, it still succeeded in showing the relevance of the musculature on the stress development in bones.

In conclusion, a method for including the effects of muscular forces in a continuum analysis of the long bones has been presented and illustrated for a simulation of gait. The approach is multi-disciplinary in nature in that it hopes to bring together the often separately researched fields of muscle mechanics, bone mechanics and motion analysis. Although the example presented in this dissertation is illustrative of the method, there are several aspects of the research which should

be improved before the model will have any real predictive value in accessing the failure properties in bone.

A list of the major improvements which would complement this dissertation follow:

- A complete validation of the model needs to be performed. It is known that EMG activities supports the use of the muscles utilized in this analysis, and that the joint torques are in qualitative agreement with other torques presented in the literature. However, issues such as the trajectory of the center of mass and the joint reaction forces should be analyzed.
- A more complex model of the body could be constructed. It would be advantageous to have a model which is capable of simulating the whole gait cycle. Another important improvement would be to break the torso segment into two segments so that the tilting of the pelvis could be incorporated into gait. There is a long list of possible complexities which could be added to make the simulated gait more representative of human gait; however, a balance should be maintained between the advantages of these complexities and the computational cost associated with their inclusion.
- Explore the implications of more complex and realistic models of musculo-tendon dynamics. In particular the effects of muscle mass, muscle viscosity, and contractile series elasticity should be examined. Modulation of these components by activation, especially the contractile series element, should be investigated.
- Incorporate additional muscle groups into the gait model. A major obstacle in this regard will be the computation of the neurological inputs required to control the model. It is anticipated that optimization techniques will be essential to this effort. A computationally efficient method called the *pseudo-inverse method* (Yamaguchi *et al.*, 1995) has recently been developed for performing dynamic optimizations of movement. This method should be explored.

- Although the above improvements would be beneficial to the analysis, the most critical improvement will be in the implementation of a more complex model of the bone. One possible direction would be to follow the work of Toridis or Rybicki and modeling the bone as a beam which is transversely isotropic. This would allow for the inclusions of shear deformations and bending. It is also a model appropriate throughout the gait cycle, so that full use could be made of the derived loading conditions. Another direction would be to treat the whole skeletal structure as a space frame. Whatever model is utilized a careful interpretation of the output of the dynamic gait model is required to correctly interpret the loading conditions that are essential in the boundary value problems.
- Characterize failure or damage in the skeletal system in terms of loading conditions associated with muscular and joint inputs. Two important issues that should be emphasized are muscle fatigue and pathological innervation. The ultimate objective of this work would be to relate critical stress to muscular failure.

## BIBLIOGRAPHY

- Audu, M.L., and Davy, D.T. (1985) The influence of muscles model complexity in musculoskeletal motion modeling. *J. Biomech. Engrg.*, 107: 147-157.
- Biewener, A.A. (1992) *Biomechanics Structures and Systems: A Practical Approach*, Oxford University Press, New York.
- Brand, R.A., Crowninshield, R.D., Wittstock, C.E., Pedersen, D.R., Clark, C.R., and Van Krieken, F.M. (1982) A model of lower extremity muscular anatomy. *J. Biomech. Engrg.*, 100: 88-92.
- Brand, R.A., Pedersen, D.R., and Friederich, J.A. (1986) The sensitivity of muscle force predictions to changes in physiologic cross-sectional area. *J. Biomech.*, 19: 589-596.
- Collier, R.J., Nadav, O., and Thomas, T.G., (1982) The mechanical resonances of a human tibia: Part I - *in vivo*. *J. Biomech.*, 15: 545-553.
- Cowin, S., Hart, R.T., and Balser, J.R., (1985) Functional Adaption in long bones: establishing *in vivo* values for surface remodeling rate coefficients. *J. Biomech.*, 18: 665-684.
- Crowninshield, R.D. (1978) Use of optimization techniques to predict muscle forces. *J. Biomech. Engrg.*, 100: 88-92.
- Crowninshield, R.D., Brand, R.A. (1981) A physiologically based criterion of muscle force prediction on locomotion. *J. Biomechanics.*, 14: 793-801.
- Currey, J.D. (1959) Differences in the tensile strength of bone of different histological types. *J. Anat.*, 93: 87-95.
- Davy, D.T., and Audu, M.L. (1987) A dynamic optimization technique for predicting forces in the swing phase of gait. *J. Biomechanics.*, 20: 187-202.
- Delp, S.L. (1990) Surgery Simulation: A computer graphics system to analyze and design musculoskeletal reconstructions of the lower extremity. *Ph.D. Dissertation*, Department of Mechanical Engineering, Stanford University, Stanford, CA.
- Delp, S.L. and Loan, J.P. (1995) A software system to develop and analyze models of musculoskeletal structures. *Computers in Biology and Medicine.*, 25: 21-34.
- Delp, S.L., Loan, J.P., Hoy, M.G., Zajac, F.E., Topp E.L., Rosen, J.M. (1990) An interactive graphics-based model of the lower extremity to study orthopaedic surgical procedures. *IEEE Transactions on Biomedical Engineering.* 37: 757-767.

- Duda, G.N., Schneider, E. and Chao, E.Y.S. (1997) Internal forces and moments in the femur during walking. *J. Biomechanics.*, **30**: 993-941.
- Friederick, J.A. and Brand, R.A. (1990) Muscle fiber architecture in the Human lower limb. *J. Biomech.* **23**: 91-95.
- Gordon, A.M., Huxley, A.F., and Julian, F.J. (1966) Tension development in highly stretched vertebrate muscle fibres. *J. Physiol.*, **184**: 143-169.
- Hardt, D.E. (1978) Determining muscle forces in the leg during normal human walking - An application and evaluation of optimization methods. *J. Biomech. Engrg.*, **100**: 72-78.
- Hatze, H. (1976) The complete optimization of human motion. *Math. Biosci.*, **28**: 99.
- Hayes, W.C., Snyder, B., Levine, B.M., and Ramaswamy, S., (1982) Stress-morphology relationships in trabecular bone of the patella. *Finite Element in Biomechanics*. John Wiley, New York. pp 223-268.
- He, J. (1988) A feedback control analysis of the neuro-musculo-skeletal control system of a cat hindlimb. *Ph.D. Dissertation*, Department of Electrical Engineering, University of Maryland.
- Hemami, H., Jaswa, V.C., and McGhee, R.B. (1975) Some alternative formulations of manipulator dynamics for computer simulation studies. *Proc. 13th Allerton Conf. on Circuit Theory*, University of Illinois, October.
- Hill, A.V. (1938) The heat of shortening and dynamic constants of muscle. *Proc. Roy. Soc. B.*, **126**: 136-195.
- Hoy, M.G., Zajac, F.E., and Gordon, M.E. (1990) A musculoskeletal model of the human lower extremity: The effects of muscle, tendon, and moment arm on the moment-angle relationship of musculotendon actuators at the hip, knee, and ankle. *J. Biomechanics.*, **23**: 157-169.
- Huskies, R. and Chao, E.Y.S. (1983) A survey of finite element analysis in orthopedic biomechanics: the first decade. *J. Biomechanics.*, **6**: 385-409.
- Inman, V.T., Ralston, H.J., and Todd, F. (1981) *Human Walking*. J.C. Lieberman (ed.), Williams & Wilkins, Baltimore, MD.
- Ju, M., Mansour, J.M. (1988) Simulation of the double limb support phase of human gait. *J. Biomech. Engrg.*, **110**: 223-229.
- Kane, T.R. and Levinson, D.A. (1985) *Dynamics: Theory and Application*. A. Murphy and M. Eichberg (eds.), McGraw-Hill, New York.
- Kane, T.R. and Levinson, D.A. (1996) *Dynamics Online: Theory and Implementation with AUTOLEV*. Online Dynamics, Inc. Sunnyvale, CA.

- Katz, B. (1939) The relation between force and speed in muscular contraction. *J. Physiol.*, **96**: 45-64.
- King, A.I. (1984) A review of biomechanical models *J. Biomech. Engrg.*, **106**: 97-104.
- Kirk, D.E. (1970) *Optimal Control Theory. An Introduction.* R.W. Newcomb (ed.), Prentice-Hall, Englewood Cliffs, NJ.
- Koch, J.C. (1917) The laws of bone architecture. *Am. J. Anat.*, **21**: 177-289.
- Lanyon, L.E., and Smith, R.N., (1970) Bone strain in the tibia during normal quadrupedal locomotion. *Acta. Ortho. Scand* **41**: 239-247.
- Lanyon, L.E., Hampson, W.G.J., Goodship, A.E., and Shah, J.S. (1974) Bone deformation recorded in vivo from strain gauges attached to the human tibia shaft. *Acta Ortho. Scand.*, **46**: 256-268.
- Lanyon, L.E. (1984) Static vs dynamics load as an influence on bone remodeling. *J. Biomechanics.*, **17**: 897-905.
- Larson, R.E., and Casti, J.L. (1978) *Principles of Dynamic Programming.* Part I. Basic Analytic and Computational Methods. J.M. Mendel (ed.), Marcel Dekker, New York.
- Levine, W.S., Christodoulou, M., Zajac, F.E. (1983) On propelling a rod to a maximum vertical or horizontal distance. *Automatica.*, **19**: 321-324.
- Markey, K.L. (1989) Stress fractures. *Clinics in Sports Medicine.*, **6**: 405-421.
- McMahon, T.A. (1984) *Muscles, Reflexes, and Locomotion*, Princeton University Press, Princeton, New Jersey.
- Pandy, M.G., and Berme, N., (1987) Synthesis of human walking: A three-dimensional model for the single support. Part 2: pathological gait. *ASME Winter Annual Meeting*, Boston, December 13-18, pp. 9-15.
- Pandy, M.G., Zajac, F.E., Sim, E., Levine, W.S. (1990) An optimal control model for maximum-height human jumping. *J. Biomechanics.*, **23**: 1185-1198.
- Patriarco, A.G., Mann, R.W., Simon, S.R., and Mansour, J.M., (1981) An evaluation of the approaches of optimization models in the prediction of muscle forces during human gait. *J. Biomechanics.*, **14**: 513-525.
- Penrod, D.D., Davy, D.T. and Singh, D.P., (1974) An optimization approach to tendon force analysis. *J. Biomechanics.*, **7**: 123-129.
- Pierrynowski, M.R., Morrison, J.B., (1985) Estimating the muscle forces generated in the human lower extremity when walking: A physiological solution. *Mathematical Biosciences.* **75**: 43-68.

- Piziali, R., Hight, T. (1976) An extended structural analysis of long bones - an application to the human tibia. *J. Biomechanics.*, 9: 695-674.
- Orne, D. and Manke, J. (1975) The influence of musculature on the mechanical impedance of the human ulna and *in vivo* simulated study. *J. Biomechanics.*, 8: 143-149.
- Otten, E. (1987) A myocybernetic model of the jaw system of the rat. *J. Neuroscience Methods.*, 21: 287-302.
- Reilly, D.T. and Burstein, A.H. (1975) The elastic and ultimate properties of compact bone tissue. *J. Biomechanics.*, 1: 393-405.
- Rybicki, E.F., Simonen, F.A. and Weis, E.B. (1972) On the mathematical analysis of stress in the human femur. *J. Biomechanics.*, 5: 203-215.
- Salathe, E.P. Jr, Arangio, G.A. and Salathe, E.P. (1989) An application of beam theory to determine the stress and deformation in long bones. *J. Biomechanics.*, 22: 189-199.
- Saunders, J.B. deC. M., Inman, V.T. and Eberhart, H.D. (1953) The major determinants in normal and pathological gait. *J. Bone Jt. Surg.*, 35-A: 543-559.
- Seireg, A., and Arvikar, R.J. (1973) A mathematical model for the evaluation of forces in the lower extremities of the musculo-skeletal system. *J. Biomechanics.*, 6: 313-326.
- Seireg, A., and Arvikar, R.J. (1975) The prediction of muscular load sharing and joint forces in the lower extremities during walking. *J. Biomechanics.*, 8: 89-102.
- Sharkey, N.A., Ferris, T.L., Smith, T.S. and Mathews D.K. (1995) Strain and Loading of the Second Metatarsal during heel-lift. *J. Bone and Joint Surgery.*, 77: 1050-1057.
- Toridis, T.G. (1969) Stress analysis of the femur. *J. Biomechanics.*, 2: 163-174.
- Thomsen, J.J. (1990) Modelling the human tibia structural vibrations. *J. Biomechanics.*, 23: 215-228.
- Viano, D., Helfenstein, M., Ankliker, M., and Ruegsegger, P. (1976) Elastic properties of corical bone in female human femurs. *J. Biomechanics.*, 9: 703-710.
- Wainwright, S.A., Biggs, W.D., Currey, J.D., and Gosline, J.M. (1972) *Mechanical design in organisms* Edward Arnold Publishers Limited, London.
- Wendt, P.P., and Johnson, R.P. (1985) A study of quadriceps excursion, torque, and the effect of patellectomy on cadaver knees. *J. Bone Jt. Surgery.*, 67-A: 726-732.

- Wickiewicz, T.L., Roy, R.R., Powell, P.L., and Edgerton, V.R. (1983) Muscle architecture of the human lower limb. *Clin. Orthop. Rel. Res.*, **179**: 275-283.
- Winter, D.A. (1979) *Biomechanics of Human Movement*. J.H. Milsum (ed.), John Wiley & Sons, New York, NY.
- Winter, D.A. (1987) *The Biomechanics and Motor Control of Human Gait*. University of Waterloo Press, Waterloo, Ontario, Canada.
- Wolff, J. (1870) Über die innere architektur der knochen und ihre bedeutung für die frage vom knochenwachstum. *Virchow's Archive*. **50**: 389-450.
- Wolff, J. (1892) *Das gesets der transformation der knochen*. Quarto, Berlen.
- Yamaguchi, G.T. (1989) Feasibility and Conceptual design of functional neuromuscular stimulation systems for the restoration of natural gait to paraplegics based on dynamic musculoskeletal models. *Ph.D. Thesis*, Department of Mechanical Engineering, Stanford University, Stanford, CA Aug. 1989.
- Yamaguchi, G.T., and Zajac, F.E. (1990) Restoring unassisted natural gait to paraplegics via functional neuromuscular stimulation: A computer simulation study. *IEEE Trans. Biomed. Engrg.*, **37**: 886-902.
- Yamaguchi, G.T., Morgan, D.W., Si, J. (1995) A computationally efficient method for solving the redundant problem in biomechanics. *J. Biomechanics*, **42**: 999-1005.
- Zajac, F.E. (1989) Muscle and tendon: Properties, models, scaling, and application to biomechanics and motor control. In *CRC Critical Reviews in Biomechanical Engineering*. **17**: 359-410.
- Zajac, F.E., and Gordon, M.E. (1989) Determining muscle's force and action in multi-articular movement. *Exercise and Sports Science Reviews*, **17**: 187-230.



APPENDIX  
AUTOLEV CODE

```

% File      : walk.al [AUTOLEV 3]
% Problem   : 7 link, 8 DOF model
% Desription : This model will have torques at all joints due to tendons,
%             and ground reaction forces on both feet. It has two
%             auxiliary coordinates to produce reaction forces at the
%             shank joints in the normal direction.
%
%             Stance-side muscles added: Soleus, Gastrocnemius, Vasti,
%             Iliopsoas, and the Gluteus Medius/Minimus.
%
%             Swing-side muscles added: Dorsiflexors, Vasti,
%             Iliopsoas, and the Gluteus Medius/Minimus.
%
%             Tendon and activation dynamics are included.
%
%             All muscle functions will be added to the C-code as
%             functions. Thus all changes to code can be applied
%             directly.
%
%             All muscle values of Yamaguchi are used explicitly.
%
%             For muscle crossing the knee, the moment arm integration
%             technique is used to figure Lmt, Vasti, Ham, Gastro. Since
%             the Gastro is biarticulate across the knee and ankle, I used
%             vector addition to find Lmt, but I did utilize the moment
%             arm data across the knee.
%
% Note      : All constants are entered.
%
% Physical Declarations: Newtonian, Frames, Particles, Bodies, Points
%
autoz on

```

newtonian N	% Newtonian reference frame
frames dd,ssft,sst,ssf,ssp	% intermediate frames
frames wwft,wwt,wwf,wwp	% intermediate frames
bodies a,b,c,d,e,f,g	% 7 link model
frames sft,st,sf,sp	% reference frame for stance muscles
frames wft,wt,wf,wp	% reference frame for swing muscles
points ab,ba,bc,cb,cd,dc	% adjoining points
points de,ed,ef,fe,fg,gf	% adjoining points
points ha,hg	% heels of stance and swing foot
points ta,tg	% toes of stance and swing foot
%-----	
% Muscle points in the stance leg	
%-----	
points so,si	% soleus
points gao,gai	% gastrocnemius
points vso,vsi,vsei	% vasti
points iso,isi,iseo	% iliopsoas
points gmso,gmsi	% gluteus medius/minimus
%-----	
% Muscle points in swing leg	
%-----	
points doo,doi,doeo	% dorsiflexors
points ho,hi	% hamstrings
points vwo,vwi,vwei	% vasti
points iwo,iwi,iweo	% iliopsoas
points gmwo,gmwi	% gluteus medius/minimus
%-----	
% Mathematical Declarations: Variables, Constants, Specified, Mass	
%-----	
variables u12'	% generalized speeds(8)
variables q8'	% generalized coordinates; derivatives
variables FS',FGA',FVS'	% Force of muscles in stance leg

```

variables FIS',FGMS'
variables FDO',FVW',FH'           % Force of muscles in swing leg
variables FIW',FGMW'
variables lmth',lmtvs',lmtvw'     % Lengths of muscles spanning the knee
constants g                        % gravity
constants w                        % total weight
constants la1,la3,lla1,lla3       % stance-leg foot
constants lb,llb                   % stance-leg shank
constants lc,llc                   % stance-leg thigh
constants ld,lld                   % trunk
constants le=lc,le=lc-llc         % swing-leg thigh
constants lf=lb,lf=lb-llb         % swing-leg shank
constants lg1=la3,lg3=la1         % swing-leg foot
constants llg1=lla3, llg3=la1-lla1
mass a=ma,b=mb,c=mc,d=md,e=me,f=mf, g=mg
inertia a, ia1,ia2,ia3            % stance-leg foot
inertia b, ib1,ib2,ib3            % stance-leg shank
inertia c, ic1,ic2,ic3            % stance-leg thigh
inertia d, id1,id2,id3            % trunk
inertia e, ie1=ic1,ie2=ic2,ie3=ic3 % swing-leg thigh
inertia f, if1=ib1,if2=ib2,if3=ib3 % swing-leg shank
inertia g, ig1=ia1,ig2=ia2,ig3=ia3 % swing-leg foot
%-----
% Geometry Relating the Segments
%-----
simprot(n,a,-2,q1)
simprot(n,b,-2,q2)
simprot(n,c,-2,q3)
simprot(n,dd,1,q4)                % pelvic list
simprot(dd,d,-2,q5)
simprot(dd,e,2,q6)
simprot(dd,f,2,q7)

```

```

simprot(dd,g,2,q8)
simprot(a,ssft,2,pi-34*pi/180)      % stance foot
simprot(ssft,sft,1,pi/2)
simprot(b,sst,-3,pi/2)               % stance tibial
simprot(sst,st,2,pi/2)
simprot(c,ssf,-3,pi/2)               % stance femoral
simprot(ssf,sf,2,pi/2)
simprot(d,ssp,-3,pi/2)               % stance pelvic
simprot(ssp,sp,2,pi/2)
simprot(d,wwp,-3,pi/2)               % swing pelvis
simprot(wwp,wp,2,pi/2)
simprot(e,wwf,3,pi/2)                % swing femoral
simprot(wwf,wf,-2,pi/2)
simprot(f,wwt,3,pi/2)                % swing tibial
simprot(wwt,wt,-2,pi/2)
simprot(g,wwft,-2,34*pi/180+pi/2)    % swing foot
simprot(wwft,wft,1,pi/2)

```

%\_\_\_\_\_

% Set up geometry for stance foot "a"

%\_\_\_\_\_

p\_ta.ab>=la1\*a1>

p\_ab\_ha>=la3\*a3>

p\_ta.ao>=lla1\*a1>+lla3\*a3> % center of mass

%\_\_\_\_\_

% Set Up Geometry for Stance Shank "b"

%\_\_\_\_\_

p\_ab.ba>=0>

p\_ba.bc>=lb\*b1>

p\_ba.bo>=llb\*b1> % center of mass

%\_\_\_\_\_

% Set Up Geometry for Stance Thigh "c"

%\_\_\_\_\_

```

p_bc.cb>=0>
p_cb.cd>=lc*c1>
p_cb.co>=llc*c1>          % center of mass
%-----
% Set Up Geometry for Stance Trunk "d"
%-----
p_cd.dc>=0>
p_dc.de>=ld*d2>
p_dc.do>=.5*ld*d2>+lld*d1>    % center of mass
%-----
% Set Up Geometry for Swing Thigh "e"
%-----
p_de.ed>=0>
p_ed.ef>=le*e1>
p_ed.eo>=lle*e1>          % center of mass
%-----
% Set Up Geometry for Swing Shank "f"
%-----
p_ef.fe>=0>
p_fe.fg>=lf*f1>
p_fe.fo>=llf*f1>          % center of mass
%-----
% Set up Geometry for Swing Foot "g"
%-----
p_fg.gf>=0>
p_gf.hg>=lg1*g1>
p_gf.tg>=lg3*g3>
p_gf.go>=llg1*g1>+llg3*g3>    % center of mass
%-----
% Soleus Stance Muscle
%-----
p_ba.so>=-.0292*st1>+.2467*st2>+.0006*st3>

```

p\_ba\_si>=-.0365\*sft1>-.0428\*sft2>+.0056\*sft3>

%

% Gastrocnemius Stance Muscle

%

p\_cb\_gao>=-.0203\*sfl>+.0071\*sf2>-.0073\*sf3>

p\_ba\_gai>=-.0368\*sft1>-.0429\*sft2>+.0028\*sft3>

%

% Vasti Stance Muscle

%

p\_cb\_vso>=.0106\*sfl>+.2026\*sf2>+.0205\*sf3>

p\_ba\_vsi>=.0170\*st1>+.3930\*st2>-.0006\*st3>

%

% Iliopsoas Stance Muscle

%

p\_cd\_iso>=.0075\*sp1>+.1350\*sp2>-.04\*sp3>

p\_bc\_isi>=-.0180\*sfl>+.3351\*sf2>+.0116\*sf3>

p\_cd\_iseo>=.0260\*sp1>+.0293\*sp2>-.0042\*sp3>

%

% Gluteus Medius Stance Muscle

%

p\_dc\_gmso>=-.0155\*sp1>+.0785\*sp2>+.0076\*sp3>

p\_cb\_gmsi>=-.0159\*sfl>+.3873\*sf2>+.0589\*sf3>

%

% Dorsiflexors Swing Muscle

%

p\_fg\_doo>=-.0155\*wt1>+.2175\*wt2>+.0134\*wt3>

p\_fg\_doi>=.1035\*wft1>-.052\*wft2>

p\_fg\_doeo>=.0259\*wt1>+.0117\*wt2>-.0093\*wt3>

%

% Hamstring Swing Muscle

%

p\_de\_ho>=-.0409\*wp1>-.0455\*wp2>-.014\*wp3>

```

p_fg_hi>=-.017*wt1>+.38*wt2>+.0073*wt3>
%-----
% Vasti Swing Muscle
%-----
p_ef_vwo>=.0106*wf1>+.2026*wf2>+.0205*wf3>
p_fg_vwi>=.0170*wt1>+.3930*wt2>-.0006*wt3>
%-----
% Iliopsoas Swing Muscle
%-----
p_de_iwo>=.0075*wp1>+.1350*wp2>-.04*wp3>
p_ef_iwi>=-.0180*wf1>+.3351*wf2>+.0116*wf3>
p_de_iweo>=.0260*wp1>+.0293*wp2>-.0042*wp3>
%-----
% Gluteus Medius Swing Muscle
%-----
p_de_gmwo>=-.0155*wp1>+.0785*wp2>+.0076*wp3>
p_ef_gmwi>=-.0159*wf1>+.3873*wf2>+.0589*wf3>
%-----
% Kinematic Differential Equations
%-----
q1'=u1
q2'=u2
q3'=u3
q4'=u4
q5'=u5
q6'=u6
q7'=u7
q8'=u8
%-----
% Angular Velocity of the Segments
%-----
w_a_n>=-q1'*n2>

```



```

w_b_n>=-q2'*n2>
w_c_n>=-q3'*n2>
w_dd_n>=q4'*n1>
w_d_dd>=-q5'*dd2>
w_d_n>=w_d_n>
w_e_dd>=q6'*dd2>
w_e_n>=w_e_n>
w_f_dd>=q7'*dd2>
w_f_n>=w_f_n>
w_g_dd>=q8'*dd2>
w_g_n>=w_g_n>
%-----
% Velocities of Points
%-----
v_ta_n>=0>
v2pts(n,a,ta,ab)
v2pts(n,a,ta,ao)
v2pts(n,a,ab,ha)
%
v_ba_n>=v_ab_n>
v2pts(n,b,ba,bo)
v2pts(n,b,ba,bc)
%
v_cb_n>=v_bc_n>
v2pts(n,c,cb,co)
v2pts(n,c,cb,cd)
%
v_dc_n>=v_cd_n>
v2pts(n,d,dc,do)
v2pts(n,d,dc,de)
%
v_ed_n>=v_de_n>

```

```

v2pts(n,e,ed,eo)
v2pts(n,e,ed,ef)
%
v_fe_n>=v_ef_n>+u9*f1>+ u10*f3>
auxiliary[1]=u9
auxiliary[2]=u10
v2pts(n,f,fe,fo)
v2pts(n,f,fe,fg)
%
v_gf_n>=v_fg_n>+u11*f1>+u12*f3>
auxiliary[3]=u11
auxiliary[4]=u12
v2pts(n,g,gf,go)
v2pts(n,g,gf,tg)
v2pts(n,g,gf,hg)
%
% Motion Constraints
%
constrain(auxiliary[u9,u10,u11,u12])
%
% Forces
%
Gravity(-g*n3>)
%
% Ground Reaction Forces and Torques at Heels
%
specified zheela',zheelg',delta'
% The following functions will needed to be added to the C-code.
specified fa3,fg1,fg3,tt
variables tabt,tbct,tcdt,tDET,teft,tfgt
Variables rfe3,rfg3
%
```

```

% The following functions will not be embedded in Z variables.
zee_not=[tabt,tbct,tcdt,tDET,teft,tfgt,fa3,fg1,fg3,tt,rfe1,rfe3,rfg1,
rfg3,FS,FGA,FVS,FIS,FGMS,FGMW,FIW,FVW,FH,FDO]
%
zheela=dot(p_ta_ha>,n3>)
zheela'=dt(zheela)
zheelg=dot(p_ta_hg>,n3>)
zheelg'=dt(zheelg)
heeln1=dot(v_hg_n>,n1>)
delta=-q8+2.164
delta'=dt(delta)
%
% Ground reaction force on stance toe.
Force_ha>+=fa3*n3>
%
% Ground reaction force on swing heel.
Force_hg>+=fg1*n1>+fg3*n3>
%
% Torque on swing foot.
Torque_g>+=tt*dd2>
%
% Passive Joint Moments
%
% The following variables specify the passive joint moments.
Constants kab4,kbc4,kcd4,kde4,kef4,kfg5
Constants theta_ab2,theta_bc2,theta_cd2
Constants theta_de2,theta_ef2,theta_fg2
Constants cab1,cbc1,ccd1,cde1,cef1,cfg1
%
% Joint angles defined.
theta_ab=q1-q2+(34*pi/180)
theta_bc=q2-q3

```

```

theta_cd=q3-q5
theta_de=pi-(q5+q6)
theta_ef=q6-q7
theta_fg=(124*pi/180)-(q8-q7)
%
% Passive torques defined.
tabt=(kab1*exp(-kab2*(theta_ab-theta_ab2))-
kab3*exp(-kab4*(theta_ab1-theta_ab))-cab1*dt(theta_ab))
tbct=(kbc1*exp(-kbc2*(theta_bc-theta_bc2))-
kbc3*exp(-kbc4*(theta_bc1-theta_bc))-cbc1*dt(theta_bc))
tcdt=(kcd1*exp(-kcd2*(theta_cd-theta_cd2))-
kcd3*exp(-kcd4*(theta_cd1-theta_cd))-ccd1*dt(theta_cd))
tdet=(kde1*exp(-kde2*(theta_de-theta_de2))-
kde3*exp(-kde4*(theta_de1-theta_de))-cde1*dt(theta_de))
teft=(kef1*exp(-kef2*(theta_ef-theta_ef2))-
kef3*exp(-kef4*(theta_ef1-theta_ef))-cef1*dt(theta_ef))
tfgt=(kfg1*exp(-kfg2*(theta_fg-theta_fg2))-
kfg3*exp(-kfg4*(theta_fg1-theta_fg))-cfg1*dt(theta_fg))
%
torque(a/b,tabt*n2>)
torque(b/c,tbct*n2>)
torque_c>-=tcdt*n2>
torque_d>+=tcdt*dd2>
torque(e/d,tdet*dd2>)
torque(f/e,teft*dd2>)
torque(g/f,tfgt*dd2>)
%
%_____
% Muscles
%_____
%
% None of the lengths nor forces are normalized.

```

```

% Constants are input.
% These functions will be specified in the C code
%
Specified fla,flp,fv,K,cs,Lt,Lm,mrv,mrh,mrg
% time constant
Constants tau
%
% Soleus muscle on stance leg
%
Specified lmtso',lmso,ltso,lwso,vmtso,vmso,vtso,csso,aso,faso,ms
Constants F0mso,L0mso,Lstso,Paso
%
ms=dot(cross(p_ab_so>,unitvec(p_so_si>)),n2>)
lwso= L0mso*sin(Paso)
lmtso=mag(p_so_si>)
vmtso=dt(lmtso)
ltso=Lstso*Lt
lmso=Lm
csso=cs
%
faso=( (FS/csso) - F0mso*flp) / ( F0mso*aso*fla )
vmso=(L0mso/tau)*fv/csso
vtso=vmtso-vmso
FS'=(F0mso/lstso)*K*(vtso)
%
torque(a/b,FS*ms*n2>)
%
% Gastrocnemius muscle on stance leg
%
Specified lmtga',lmga,ltga,lwga,vmtga,vmga,vtga,csga,aga,faga,mgak,mgaa
Constants F0mga,L0mga,Lstga,Paga
%
```

```

mgak=-mrg*(q3-q2)
mgaa=dot(cross(p_ab_gao>,unitvec(p_gao_gai>)),n2>)
lwga=L0mga*sin(Paga)
lmtga=mag(p_gao_gai>)
vmtga=dt(lmtga)
ltga=Lstga*Lt
lmga=Lm
csga=cs
%
faga=((FGA/csga)-F0mga*flp)/(F0mga*aga*fla)
vmga=(L0mga/tau)*fv/csga
vtga=vmtga-vmga
FGA'=(F0mga/Lstga)*K*(vtga)
%
torque(a/b,FGA*mgaa*n2>)
torque(b/c,FGA*mgak*n2>)
%
% Vasti muscle on stance leg
%
Specified lmvs,ltvs,lwvs,vmtvs,vmvs,vtvs,csvs,avs,favs,mvs
Constants F0mvs,L0mvs,Lstvs,Pavs
%
mvs=mrV*(q3-q2)
lwvs=L0mvs*sin(Pavs)
lmtvs'=mrV*(q3-q2)*(u3-u2)
vmtvs=lmtvs'
ltvs=Lstvs*Lt*(lmtvs-lmvs)
lmvs=Lm
csvs=cs
%
favs=((FVS/csvs)-F0mvs*flp)/(F0mvs*avs*fla)
vmvs=(L0mvs/tau)*fv/csvs

```

```

vtvs=vmtvs-vmvs
FVS'=(F0mvs/Lstvs)*K*(vtvs)
%
torque(b/c,FVS*mvs*n2>)
%
% Iliopsoas muscle on stance leg
%
Specified lmtis',lmis,ltis,lwis,vmtis,vmis,vtis,csis,ais,fais
Specified misdd1,misdd2,misn2
Constants F0mis,L0mis,Lstis,Pais
%
misdd2=dot(cross(p_cd_iseo>,unitvec(p_iseo_isi>)),dd2>)
misdd1=dot(cross(p_cd_iseo>,unitvec(p_iseo_isi>)),dd1>)
misn2=dot(cross(p_cd_iseo>,unitvec(p_iseo_isi>)),n2>)
lwis=L0mis*sin(Pais)
lmtis=(mag(p_iso_iseo>)+mag(p_iseo_isi>))
vmtis=dt(lmtis)
ltis=Lstis*Lt
lmis=Lm
csis=cs
%
fais=((FIS/csis)-F0mis*flp)/(F0mis*AIS*fla)
vmis=(L0mis/tau)*fv/csis
vtis=vmtis-vmis
FIS'=(F0mis/lstis)*K*(vtis)
%
torque_c>+=-FIS*misn2*n2>
torque_d>+=FIS*misdd2*dd2>
torque_d>+=FIS*misdd1*dd1>
%
% Gluteus Medius/Minimus muscle on stance leg
%
```

```

Specified lmtgms',lmgms,ltgms,lwgmms,vmtgms,vmgmms,vtgmms
Specified csgmms,agmms,fagmms
Specified mgmmsdd2,mgmmsdd1,mgmmsn2
Constants F0mgmms,L0mgmms,Lstgmms,Pagmms
%
mgmmsdd2=dot(cross(p.cd_gmso>,unitvec(p_gmso_gmsi>)),dd2>)
mgmmsdd1=dot(cross(p.cd_gmso>,unitvec(p_gmso_gmsi>)),dd1>)
mgmmsn2=dot(cross(p.cd_gmso>,unitvec(p_gmso_gmsi>)),n2>)
lwgmms=L0mgmms*sin(Pagmms)
lmtgmms=mag(p_gmso_gmsi>)
vmtgmms=dt(lmtgmms)
ltgmms=Lstgmms*Lt
lmgmms=Lm
csgmms=cs
%
fagmms=((FGMS/csgmms)-F0mgmms*flp)/(F0mgmms*AGMS*fla)
vmgmms=(L0mgmms/tau)*fv/csgmms
vtgmms=vmtgmms-vmgmms
FGMS'=(F0mgmms/lstgmms)*K*(vtgmms)
%
torque.c>+=-FGMS*mgmmsn2*n2>
torque.d>+=FGMS*mgmmsdd2*dd2>
torque.d>+=FGMS*mgmmsdd1*dd1>
%
% Dorsiflexors muscles on swing leg
%
Specified lmtdo',lmdo,ltdo,lwdo,vmtdo,vmdo,vtdo,csdo,ado,fado,mdo,fsdo
Constants F0mdo,L0mdo,Lstdo,Pado
%
mdo=dot(cross(p_fg_doeo>,unitvec(p_doeo_doi>)),dd2>)
lwdo=L0mdo*sin(Pado)
lmtdo=(mag(p_doo_doeo>)+mag(p_doeo_doi>))

```



```

vmtdo=dt(lmtdo)
ltdo=Lstdo*Lt
lmdo=Lm
csdo=cs
%
fado=((FDO/csdo)-F0mdo*flp)/(F0mdo*ADO*fla)
vmdo=(L0mdo/tau)*fv/csdo
vtdo=vmtdo-vmdo
FDO'=(F0mdo/Lstdo)*K*(vtdo)
%
fsdo=(FDO)*dot(f1>,unitvec(p_doeo_doi>))
%
torque(g/f,FDO*mdo*dd2>)
%
% Hamstring muscle in swing leg
%
Specified lmh,lth,lwh,vmth,vmh,vth,csh,ah,fah,mhk,mhh,fsh
Constants F0mh,L0mh,Lsth,Pah
%
mhk=mrh*(q7-q6)
mhh=dot(cross(p_de_ho>,unitvec(p_ho_hi>)),dd2>)
lwh=L0mh*sin(Pah)
lmth'=mrh*(q7-q6)*(u7-u6)
vmth=lmth'
lth=Lsth*Lt*(lmth-lm)
lmh=Lm
csh=cs
%
fah=((FH/csh)-F0mh*flp)/(F0mh*AH*fla)
vmh=(L0mh/tau)*fv/csh
vth=vmth-vmh
FH'=(F0mh/Lsth)*K*(vth)

```

```

%
fsh=FH*dot(f1>,unitvec(p_ho_hi>))
%
torque(f/e,FH*mhk*dd2>)
torque(e/d,FH*mhh*dd2>)
%
% Vasti muscle on swing leg
%
Specified lmvw,ltvw,lwvw,vmtvw,vmvw,vtvw,csvw,avw,favw,mvw,fsvw
Constants F0mvw,L0mvw,Lstvw,Pavw
%
mvw=mrw*(q7-q6)
lwvw=L0mvw*sin(Pavw)
lmtvw'=mrw*(q7-q6)*(u7-u6)
vmtvw=lmtvw'
ltvw=Lstvw*Lt*(lmtvw-lmvw)
lmvw=Lm
csvw=cs
%
favw=((FVW/csvw)-F0mvw*flp)/(F0mvw*avw*fla)
vmvw=(L0mvw/tau)*fv/csvw
vtvw=vmtvw-vmvw
FVW'=(F0mvw/Lstvw)*K*(vtvw)
%
fsvw=FVW*dot(f1>,unitvec(p_vwo_vwi>))
%
torque(f/e,FVW*mvw*dd2>)
%
% Iliopsoas muscle on swing leg
%
Specified lmtiw',lmiw,ltiw,lwiw,vmtiw,vmiw,vtiw,csiw,aiw,faiw,miw
Constants F0miw,L0miw,Lstiw,Pairw

```

```

%
miw=dot(cross(p_de_iweo>,unitvec(p_iweo_iwi>)),dd2>)
lwi=L0miw*sin(Paiw)
lmtiw=(mag(p_iwo_iweo>)+mag(p_iweo_iwi>))
vmtiw=dt(lmtiw)
ltiw=Lstiw*Lt
lmiw=Lm
csiw=cs
%
faiw=((FIW/csiw)-F0miw*flp)/(F0miw*AIW*fla)
vmiw=(L0miw/tau)*fv/csiw
vtiw=vmtiw-vmiw
FIW'=(F0miw/Lstiw)*K*(vtiw)
%
torque(e/d,FIW*miw*dd2>)
%
% Gluteus Medius/Minimus muscle on swing leg
%
Specified lmtgmw',lmgmw,ltgmw,lwgmw,vmtgmw,vmgmw,vtgmw
Specified csgmw,agmw,fagmw,mgmw
Constants F0mgmw,L0mgmw,Lstgmw,Pagmw
%
mgmw=dot(cross(p_de_gmwo>,unitvec(p_gmwo_gmwi>)),dd2>)
%
lwgmw=L0mgmw*sin(Pagmw)
lmtgmw=mag(p_gmwo_gmwi>)
vmtgmw=dt(lmtgmw)
ltgmw=Lstgmw*Lt
lmgmw=Lm
csgmw=cs
%
fagmw=((FGMW/csgmw)-F0mgmw*flp)/(F0mgmw*AGMW*fla)

```

```

vmgmw=(L0mgmw/tau)*fv/csgmw
vtgmw=vmtgmw-vmgmw
FGMW'=(F0mgmw/Lstgmw)*K*(vtgmw)
%
torque(e/d,FGMW*mgmw*dd2>)
%
% Forces at the ankle and knee of the swing side shank
%
Force(ef/fe,rfe1*f1>+rfe2*f2>+rfe3*f3>)
Force(fg/gf,rfg1*f1>+rfg2*f2>+rfg3*f3>)
%
Contributions=fr()
%
% Segmental Torques
%
torque_a>
torque_b>
torque_c>
torque_d>
torque_e>
torque_f>
torque_g>
%
% Equations of Motion
%
zero=fr()+frstar()
kane(rfe1,rfe3,rfg1,rfg3)
%
% Expression to be Output by the C Code
%
output T,q1
output T,q2

```

```

output T,q3
output T,q4
output T,q5
output T,q6
output T,q7
output T,q8
output etc.
%-----
% Units Constants for C Code
%-----
units [t]=s
units [tau]=s
units [q1,q2,q3,q4,q5,q6,q7,q8]=deg
units [u1,u2,u3,u4,u5,u6,u7,u8]=r/s
units [FS,FGA,FVS,FIS,FGMS,FDO,FVW,FH,FIW,FGMW]=N
units [la1,la3,lla1,lla3,lb,lb,lc,lc,ld,ld]=m
units [ma,mb,mc,md,me,mf,mg,w]=kg
units [ia1,ia2,ia3,ib1,ib2,ib3,ic1,ic2,ic3,id1,id2,id3]=kg*m2
units [cab1,cbc1,ccd1,cde1,cef1,cfg1]=(N*s)/(r*m)
units [kab1,kab3,kbc1,kbc3,kcd1,kcd3,kde1,kde3,kef1,kef3,kfg1,kfg3]=N*m
units [kab2,kab4,kbc2,kbc4,kcd2,kcd4,kde2,kde4,kef2,kef4,kfg2,kfg4]=1/r
units [theta_ab1,theta_ab2,theta_bc1,theta_bc2,theta_cd1,theta_cd2]=r
units [theta_de1,theta_de2,theta_ef1,theta_ef2,theta_fg1,theta_fg2]=r
units [g]=m/s2
units [F0mSo,F0mGA,F0mVS,F0mIS,F0mGMS]=N
units [F0mDO,F0mVW,F0mH,F0mIW,F0mGMW]=N
units [L0mSo,L0mGA,L0mVS,L0mIS,L0mGMS]=m
units [L0mDO,L0mVW,L0mH,L0mIW,L0mGMW]=m
units [LstSo,LstGA,LstVS,LstIS,LstGMS]=m
units [LstDO,LstVW,LstH,LstIW,LstGMW]=m
units [PaSo,PaGA,PaVS,PaIS,PaGMS]=deg
units [PaDO,PaVW,PaH,PaIW,PaGMW]=deg

```

```

input g=9.81
input ia1=.002,ia2=.008,ia3=.009,ib1=.019,ib2=.065,ib3=.065
input ic1=.080,ic2=.126,ic3=.126,id1=.764,id2=3.407,id3=3.297
input la1=.175,la3=.118,lb=.435,lc=.410,ld=.172,lla1=.1,lla3=.0295
input llb=.247,llc=.227,lld=.343,ma=1.1,mb=3.75,mc=7.58,md=51.22
input me=7.58,mf=3.75,mg=1.1
input cab1=.943,cbc1=3.17,ccd1=1.09,cde1=1.09,cef1=3.17,cfg1=.943
input kab1=2,kab2=5,kab3=9,kab4=5
input kbc1=3.1,kbc2=5.9,kbc3=10.5,kbc4=11.8
input kcd1=2.6,kcd2=5.8,kcd3=8.7,kcd4=1.3
input kde1=2.6,kde2=5.8,kde3=8.7,kde4=1.3
input kef1=3.1,kef2=5.9,kef3=10.5,kef4=11.8
input kfg1=2,kfg2=5,kfg3=9,kfg4=5
input theta_ab1=1.92,theta_ab2=1.047,theta_bc1=0,theta_bc2=-1.92
input theta_cd1=1.92,theta_cd2=.1744,theta_de1=1.92,theta_de2=.1744
input theta_ef1=0,theta_ef2=-1.92,theta_fg1=1.92,theta_fg2=1.047
input F0mso=3599,L0mso=.0243,Lstso=.27,Paso=25
input F0mga=1423,L0mga=.0482,Lstga=.4250,Paga=14.8
input F0mvs=6482,L0mvs=.1096,Lstvs=.2250,Pavs=4.5
input F0mis=1474,L0mis=.1269,Lstis=.0850,Pais=7
input F0mgms=2686,L0mgms=.0760,Lstgms=.0355,Pagms=10.4
input F0mdo=1400,L0mdo=.1009,Lstdo=.2250,Pado=6.9
input F0mvw=6482,L0mvw=.1096,Lstvw=.2250,Pavw=4.5
input F0mh=2348,L0mh=.1065,Lsth=.3850,Pah=8.7
input F0miw=1474,L0miw=.1269,Lstiw=.0850,Paiw=7
input F0mgmw=2686,L0mgmw=.0760,Lstgmw=.0355,Pagmw=10.4
input tinitial=0,tfinal=.6,integstp=.01

```

---

```

%
% C Code generation for numerical solution
digits 6
code dynamics() walk.c, subs

```